Photoinduced, Copper-Catalyzed Alkylation of Amines: A Mechanistic Study of the Cross-Coupling of Carbazole with Alkyl Bromides

Jun Myun Ahn,[†] Tanvi S. Ratani,[†] Kareem I. Hannoun, Gregory C. Fu,* and Jonas C. Peters*

Division of Chemistry and Chemical Engineering, California Institute of Technology, Pasadena, California 91125, United States

Supporting Information

Table of Contents

I. General information

Chemicals. Unless otherwise noted, all materials were purchased from commercial suppliers and used as received. All manipulations of air-sensitive materials were carried out in oven-dried glassware using standard Schlenk or glovebox techniques under an N_2 atmosphere. Solvents were deoxygenated and dried by thoroughly sparging with argon followed by passage through an activated column in a solvent purification system. Silicycle *Silia*Flash® P60 Silica gel (particle size 40–63 nm) was used for flash chromatography. Analytical thin layer chromatography was conducted with glass TLC plates (silica gel 60 F254) and spots were visualized under UV light or after treatment with standard TLC stains. Carbazole (carbH) was recrystallized from hot ethanol. Mesitylcopper[1] and 2-bromo-4-phenylbutane,[2] were prepared following a reported procedure. Note: herein carbazolide = carb and they are used interchangeably.

EPR, Infrared, and UV-vis Spectroscopy. X-band EPR measurements were made with a Bruker EMX spectrometer at 77 K. Simulation of EPR data was conducted using the software EasySpin.[3] IR measurements were recorded on a Bruker ALPHA Diamond ATR. Absorbance spectra were acquired on a Cary 50 UV-vis spectrophotometer with a Unisoku Scientific Instruments cryostat to maintain temperature.

NMR spectroscopy. ^{1}H, ^{2}H, ^{13}C, ^{7}Li, ^{31}P NMR, and DOSY spectra were recorded on a Bruker Ascend 400, a Varian 300 MHz, a Varian 400 MHz, a Varian 500 MHz, or a Varian 600 MHz spectrometer, and referencing was done using either the proteo impurity in a deuterated solvent, or to the deuterium lock signal. Multiplicity and qualifier abbreviations are as follows: s = singlet, d = doublet, t = triplet, q = quartet, m = multiplet, br = broad, app = apparent.

Gas chromatography. Calibrated GC yields were obtained on an Agilent 6890 Series system with an HP-5 column (length 30 m, I.D. 0.25 mm, FID Detector) using dodecane as an internal standard.

X-ray crystallography. XRD studies were carried out at the Beckman Institute Crystallography Facility (http://www.its.caltech.edu/~xray/index.html) on a Bruker D8 Venture kappa duo photon 100 CMOS instrument (Mo Kα radiation). Structures were solved using SHELXT and refined against F^2 by full-matrix least squares with SHELXL and OLEX2. Hydrogen atoms were added at calculated positions and refined using a riding model. The crystals were mounted on a glass fiber or a nylon loop with Paratone N oil.

Photolytic reactions. Photolytic reactions were performed using a 100-W Blak-Ray Long Wave Ultraviolet Lamp (Hg), 100-W Blak-Ray B-100Y High Intensity Inspection Lamp (Hg), or a Luzchem LZC-4V photoreactor equipped with LZC-UVA lamps centered at 350 nm (Figure S1). Temperature control was maintained with an isopropanol bath cooled by an SP Scientific cryostat. For reactions using mercury lamps, the light source was placed approximately 20 cm above the sample and the reaction mixture was stirred vigorously using a magnetic stir bar.

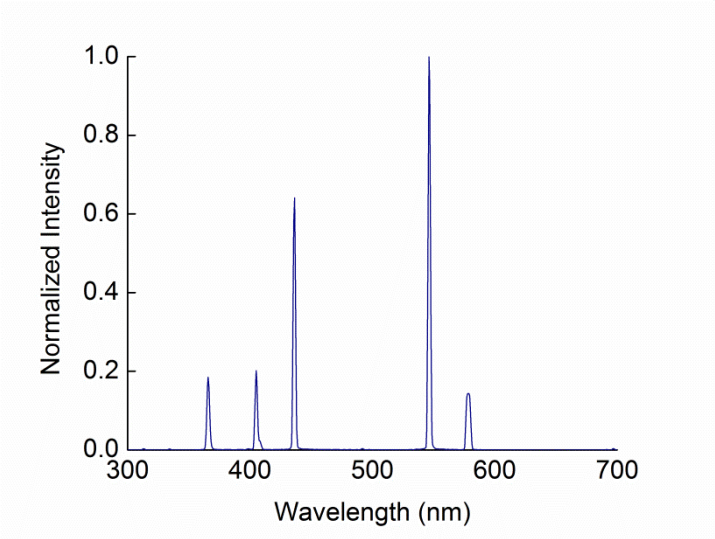

Figure S1: Emission spectrum of 100-W Blak-Ray Long Wave Ultraviolet Lamp

Photophysical methods. Steady-state fluorimetry and time-resolved transient absorption and luminescence measurements were performed in the Beckman Institute Laser Resource Center (BILRC; California Institute of Technology). Samples for room temperature transient absorption and luminescence measurements were prepared in dry (passage through alumina three times), degassed (three freeze-pump-thaw cycles) acetonitrile inside a nitrogen-filled glovebox, and transferred to a 1-cm or 1-mm pathlength fused quartz or glass cuvette (Starna Cells) which was sealed with a high-vacuum Teflon valve (Kontes), or a Harrick demountable liquid flow cell (DLC-S25) with quartz windows and 100 μm path length Teflon spacers. Steady-state emission spectra were collected on a Jobin S4 Yvon Spec Fluorolog-3-11 with a Hamamatsu R928P photomultiplier tube detector with photon counting.

For luminescence and transient absorption at the nanosecond to microsecond time scale, a Q-switched Nd:YAG laser (Spectra-Physics Quanta-Ray PRO-Series; 355 nm; pulse duration 8 ns, operating at 10 Hz) was used as the source of the excitation pulse, with laser power at 0.5 mJ/pulse. Probe light for transient absorption kinetics measurements was provided by a 75-W arc lamp (PTI Model A 1010) which was operated in continuous wave or pulsed modes. The laser light was aligned so as to be collinear with the arclamp beam, and the scattered excitation light was rejected with appropriate long pass and short pass filters. Transmitted light from the sample was detected with a photomultiplier tube (Hamamatsu R928). All instruments and electronics in these systems were controlled by software written in LabVIEW (National Instruments).

Transient absorption difference spectra were collected using the same excitation source (λ_{ex} = 355 nm), and a white light flash lamp source with nanosecond durations. All instruments and electronics in these systems were controlled by software written in LabVIEW (National Instruments). Data manipulation was performed with MatlabR2014B.

Fluorescence decay measurements at the picosecond time scale were performed as previously described.[4] A mode-locked Nd:YAG laser (Vanguard 2000-HM532; Spectra-Physics) provided 10 ps pulses that were regeneratively amplified (Continuum) and frequency tripled (355 nm excitation). Laser power was reduced to 0.5 mJ/pulse. Fluorescence from the sample was focused onto the entrance slit of a spectrograph (Acton Research Corp SpectraPro 275) through a 355 nm dielectric mirror to reject scattered excitation light. Fluorescence decays were obtained at a spectrograph center wavelength of 420 nm. Decays were collected using a streak camera (C5680; Hamamatsu Photonics) in photon counting mode over a 50 ns window. Samples were prepared in the glove box using a flow cell apparatus with quartz windows to allow for UV penetration. A sample path length of 100 μm was used by inserting Teflon spacers in between the two quartz windows. A syringe pump was used to flow sample in between two gas-tight 10 mL syringes (Hamilton) under inert atmosphere.

II. Preparation of substrates

Yields have not been optimized.

6-bromohept-1-ene [38334-98-4]:

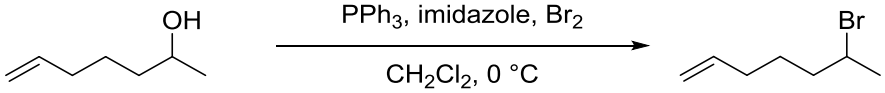

A 500 mL round-bottomed flask was charged with triphenylphosphine (14.5 g, 55 mmol), imidazole (3.7 g, 55 mmol), and a magnetic stir bar. CH_2Cl_2 (300 mL) was added under a nitrogen atmosphere and the mixture was cooled to 0 °C. Br_2 (2.6 mL, 51 mmol) was added dropwise. The resulting mixture was stirred for 30 minutes at 0 °C before a solution of hept-6-en-2-ol[5] (5 g, 44 mmol) in 10 mL CH_2Cl_2 was added dropwise at 0 °C. The mixture was stirred at 0 °C for 2 hours and allowed to warm to ambient temperature overnight. The mixture was concentrated under reduced pressure on a rotary evaporator to an approximate volume of 25 mL, and diluted with hexanes. The resulting solid was filtered, and the filtrate was concentrated and purified by column chromatography (hexanes) to yield 6.1 g (78 % yield) of colorless liquid. Spectroscopic data match those reported in the literature.[6]

(E)-6-bromohept-1-ene-1-*d*:

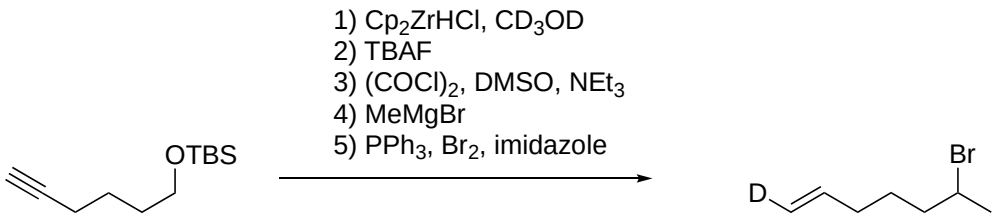

In the glovebox under nitrogen atmosphere, Cp_2ZrHCl (12 g, 47 mmol) was suspended in THF (200 mL) in a 500 mL round-bottomed flask. *tert*-butyl(hex-5-yn-1-yloxy)dimethylsilane (8.7 g, 41 mmol) in THF was then added dropwise to the stirring suspension at ambient temperature. After overnight stirring, excess D_2O (9 mL) was added to the brown solution in one portion at ambient temperature via syringe. The resulting yellow solution was allowed to stir at ambient temperature for 6 h and diluted with Et_2O (~ 250 mL). The suspension was filtered through a pad of silica over $MgSO_4$, and concentrated under reduced pressure on a rotary evaporator. The oily residue was dissolved in anhydrous THF. This solution was added to a solution of tetrabutylammonium fluoride (30 mL, 1 M in THF) at ambient temperature over 5 min. After stirring for 2 h, the mixture was extracted with diethyl ether and washed with water (50 mL). The organic layer was dried over Na_2SO_4, filtered and concentrated on a rotary evaporator. The oily residue was passed through a plug of silica gel eluting with diethyl ether, and the material with the same rf value on the TLC plate as the commercially available hex-5-en-1-ol was collected. The ^1H NMR spectrum of the oil matched that of hex-5-en-1-ol except for the resonances corresponding to the deuterated vinylic proton. The filtrate was concentrated under reduced

pressure on a rotary evaporator. The residue was dissolved in dichloromethane (10 mL). In a separate flask, DMSO (5.7 mL) in dichloromethane (5 mL) was added dropwise to a cold solution of oxalyl chloride (4.1 mL) in dichloromethane (150 mL) at –78 °C. After stirring for 15 min, the dichloromethane solution of the oily residue was added dropwise. Excess trimethylamine (28 mL) was added after 1 h at 78 °C, and the mixture was allowed to warm to ambient temperature. 1 M $HCl_{(aq)}$ (100 mL) was added to the mixture, and the aqueous layer was extracted with dichloromethane (2 x 50 mL). The organic layer was dried over Na_2SO_4, filtered, and concentrated on a rotary evaporator. The oily residue was dissolved in anhydrous Et_2O and added slowly to a cold solution of methylmagnesium bromide (20 mL, 3 M in Et_2O at –10 °C). The solution was allowed to warm to room temperature overnight and quenched with $NH_4Cl_{(aq)}$. The aqueous layer was extracted with Et_2O (2 x 50 mL), and the organic layer was dried over Na_2SO_4, filtered, and concentrated under reduced pressure on a rotary evaporator. The crude material was purified by column chromatography (70% Et_2O/hexanes), affording 2 g of colorless oil that had the same rf value on the TLC plate as hept-6-en-2-ol. The ^{1}H NMR spectrum of the oil matched that of hept-6-en-2-ol except for the resonances corresponding to the deuterated vinylic proton. This oil was subjected to the standard bromination conditions using triphenylphosphine (5.8 g), imidazole (1.5 g), and bromine (1 mL) to yield 1.2 g of (E)-6-bromohept-1-ene-1-d as colorless oil (16% yield over 5 steps). The ^{2}H NMR spectrum of this material shows approximately 9.5:1 selectivity of hydrozirconation versus over-reduction of the alkyne. The hydrozirconation proceeded in 13:1 selectivity to afford the desired *E*-isotopomer.

^{1}H NMR (300 MHz, Chloroform-*d*): δ 5.96–5.71 (m, 1H), 5.03–4.96 (m, 1H), 3.86–3.73 (m, 1H), 2.11–1.97 (m, 2H), 1.40–1.49 (m, 4H), 1.19 (d, J = 6.2 Hz, 3H).
^{13}C NMR (75 MHz, Chloroform- *d*): δ 138.08, 114.64 (t), 51.58, 40.47, 32.96, 26.96, 26.46.
^{2}H NMR (61 MHz, Chloroform): δ 5.01.
MS (EI) m/z (M-Br^+) calc for $C_7H_{12}DBr$: 98, found: 98.

III. Procedures for photoinduced cross-couplings

General procedure for the coupling of alkyl bromides

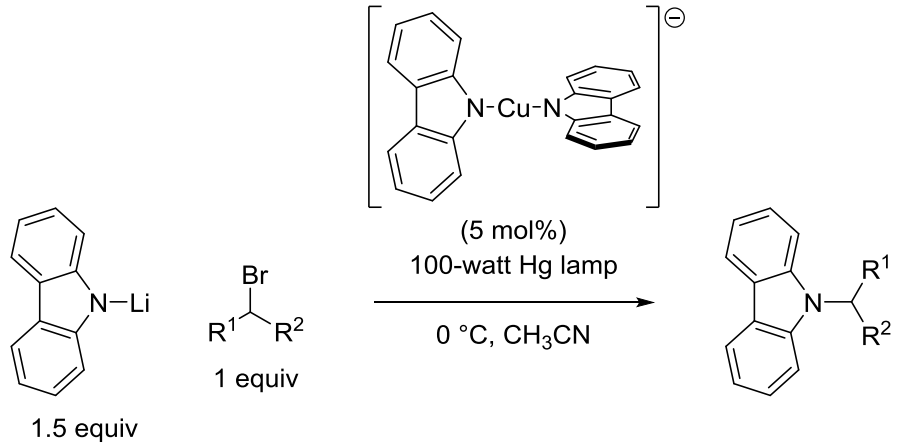

$[Li(MeCN)_n][Cu(carbazolide)_2]$ (0.0067 mmol), lithium carbazolide (0.2 mmol), and alkyl bromide (0.13 mmol) were added to a 4 mL borosilicate vial in the glovebox under a nitrogen atmosphere. A magnetic stir bar and 4 mL acetonitrile were added to the vial. The mixture was capped and stirred for 5 minutes and the reaction vessel was fully submerged in an isopropanol bath kept at 0 °C with a cryostat. The mixture was irradiated with a 100-watt Hg lamp while stirring for 8 hours, after which time it was diluted with a solution of dodecane in diethyl ether or ethyl acetate. An aliquot was filtered through a short pad of silica gel (ethyl acetate eluent) and the sample was injected for GC analysis. Products were isolated after removing the solvent *in vacuo* and loading the crude on silica gel and eluting with hexanes.

Procedure for the photolytic reaction in the absence of copper

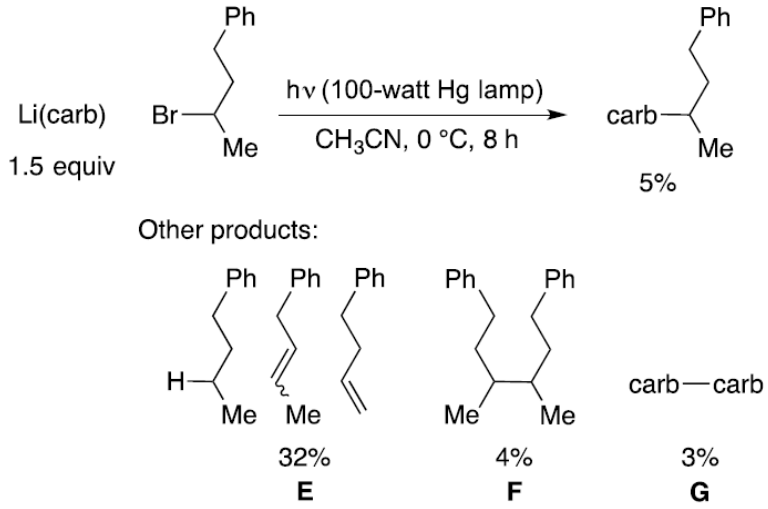

Lithium carbazolide (0.2 mmol) and alkyl bromide (0.13 mmol) were added to a 4 mL borosilicate vial in the glovebox under nitrogen atmosphere. A magnetic stir bar and 4 mL acetonitrile were added to the vial. The mixture was capped and stirred for 5 minutes and the

reaction vessel was fully submerged in an isopropanol bath kept at 0 °C with a cryostat. The mixture was irradiated with 100-watt Hg lamp while stirring for 8 hours, after which time it was diluted with a solution of dodecane in diethyl ether or ethyl acetate. An aliquot was filtered through a short pad of silica gel (ethyl acetate eluent) and the sample was analyzed by GC. Typical calibrated GC yields of products are shown in the scheme above. 9,9'-bicarbazyl (1.2 mg, 3% yield) was quantified by preparative TLC with hexanes.

Procedure for standard photolytic reactions at varying reaction concentrations

Stock solutions of $[Li(MeCN)_n][Cu(carbazolide)_2]$, lithium carbazolide, and 6-bromohept-1-ene were prepared in acetonitrile. Desired amounts of each were transferred to a 4 mL borosilicate vial, and the mixture was diluted to a total volume of 4 mL with acetonitrile. The vial was subjected to the standard photolytic conditions, and the products were analyzed by GC. Five reaction concentrations were tested: 0.011 M, 0.022 M, 0.033 M, 0.044 M, and 0.055 M in a total of 4 mL of acetonitrile using 6-bromohept-1-ene as the limiting reagent. The data are summarized in the table below. **H**/**I** values were calculated prior to rounding of yields of products **H** and **I**.

Table S1: Variation of yields of H and I as a function of alkyl bromide concentration.

Alkyl bromide [mM]	Product H (dr)	Product I	H/I
11	70% (4:1)	6.7%	11
22	68% (4:1)	9.1%	7.6
33	62% (4:1)	10%	6.1
44	55% (4:1)	10%	5.5
55	51% (4:1)	10%	5.1

Procedure for stoichiometric coupling of $[Cu^{I}(carb)_2]Li$* with 2-bromo-4-phenylbutane (Eq 4 in the main text of the published article)

Stock solutions (0.0067 mmol/mL) of $[Li(MeCN)_n][Cu(carbazolide)_2]$ and 2-bromo-4-phenybutane were prepared in acetonitrile. Then, 0.0067 mmol of each reactant was added to a 4 mL vial containing a magnetic stir bar. The mixture was diluted to a total of 4 mL with acetonitrile. The mixture was capped and stirred for 5 minutes and the reaction vessel was fully submerged in an isopropanol bath kept at 0 °C with a cryostat. The mixture was irradiated with 100-watt Hg lamp while stirring for 8 hours, after which time it was diluted with a solution of dodecane in diethyl ether or ethyl acetate. An aliquot was filtered through a short pad of silica

gel (ethyl acetate eluent) and the sample was analyzed by GC. Run 1: 95% yield. Run 2: 96% yield.

Procedure for the time-course analysis of reactions with and without [Li(MeCN)$_n$][Cu(carbazolide)$_2$]

Stock solutions of [Li(MeCN)$_n$][Cu(carbazolide)$_2$], lithium carbazolide, and 2-bromo-4-phenylbutane were prepared in acetonitrile. Desired amounts of each were transferred to a 4 mL borosilicate vial as outlined in the general procedure, and the vial was diluted to a total of 4 mL with acetonitrile. The vial was subjected to the standard photolytic conditions for the specified amount of time, and the products were analyzed by GC.

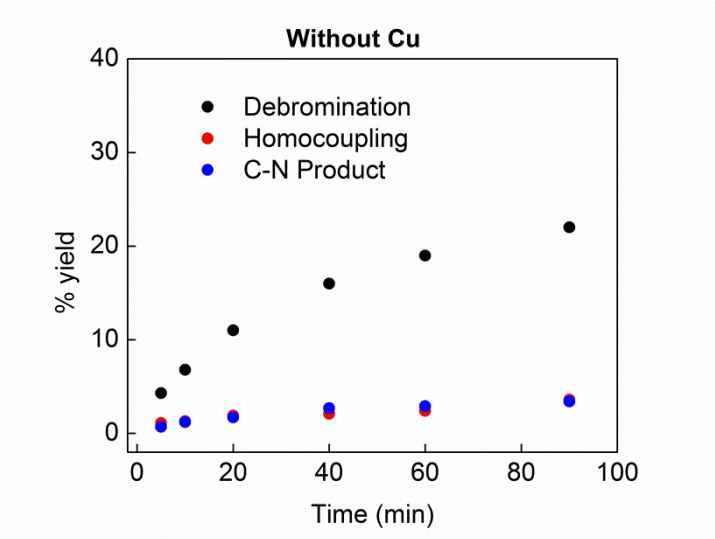

Figure S2: Time-course analysis of the standard reaction mixture in the absence of Cu.

Table S2: Yields of debromination, homocoupling, and C–N cross-coupled product over time in the absence of Cu.

Time (min)	Debromination (%)	Homocoupling (%)	C-N cross-coupled product (%)
5	4.3	1.1	0.7
10	6.8	1.3	1.2
20	11	1.9	1.7
40	16	2.1	2.7
60	19	2.4	2.9
90	22	3.6	3.4

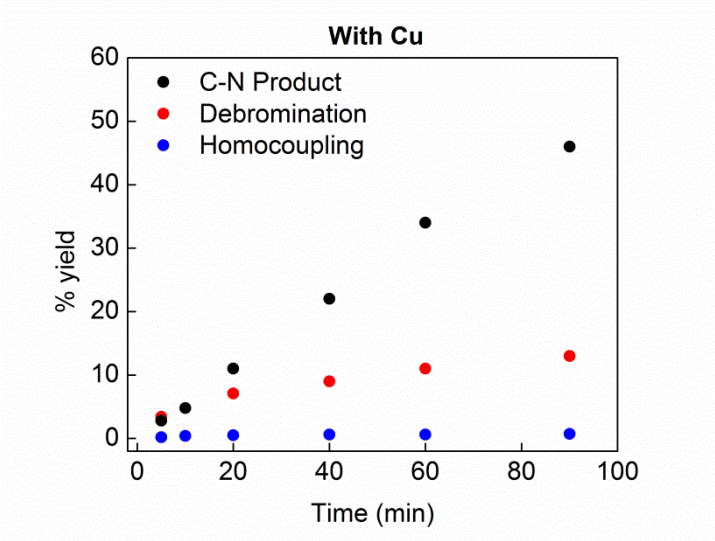

Figure S3: Time-course analysis of the standard catalysis reaction mixture.

Table S3: Yields of debromination, homocoupling, and C–N cross-coupled product over time under catalysis conditions.

Time (min)	Debromination (%)	Homocoupling (%)	C-N cross-coupled product (%)
5	3.4	0.2	2.8
10	4.8	0.4	4.8
20	7.1	0.5	11
40	9	0.6	22
60	11	0.6	34
90	13	0.7	46

IV. Preparation of metal carbazolides

Preparation of $[Li(MeCN)_n][Cu(carbazolide)_2]$

Mesitylcopper (183 mg, 1 mmol), carbazole (167 mg, 1 mmol), and lithium carbazolide (1 mmol) were added to a 20 mL scintillation vial in a nitrogen atmosphere glovebox. 10 mL of acetonitrile was added to the vial, and the mixture was stirred overnight at ambient temperature. The solution was filtered through a pad of Celite and the volatiles were removed *in vacuo*. Benzene (1 mL) was added to dissolve the oil and the residue was triturated with pentane (5 mL). The supernatant was decanted and benzene was added again. Benzene (1 mL) was added to the solid residue followed by pentane (5 mL) to precipitate the product. This process was repeated until a free-flowing, off-white powder was obtained. This powder was isolated atop a sintered glass frit and washed with benzene (3 x 5 mL) and pentane (3 x 5 mL). The title compound can be further dried under vacuum overnight to yield the title compound (400 mg) as an acetonitrile adduct as determined by ^{1}H NMR analysis. Spectroscopic data match the literature report.[7]

Preparation of Li(carbazolide) (13390-92-6)

Carbazole (3.6 g, 22 mmol) was suspended in 150 mL of diethyl ether in a 250 mL flask in a nitrogen-atmosphere glovebox. After cooling to –78 °C, butyllithium (1.6 M in hexanes, 15 mL) was added dropwise. The mixture was stirred at –78 °C for 3 h and allowed to warm to room temperature overnight. The white solid was collected atop a sintered glass frit, washed with cold diethyl ether and pentane and then recrystallized in cold THF. The crystals were then dissolved in minimal acetonitrile and the solution was dried *in vacuo* to afford the title compound (2.9 g, 76% yield). Spectroscopic data match those reported in the literature.[8]

Preparation of $[K(benzo\text{-}15\text{-}crown\text{-}5)_2][Cu^{II}(carbazolide)_3]$

A –70 °C suspension of $Cu(OTf)_2$ (36 mg, 0.05 mmol) in 2 mL THF was added dropwise to a pre-chilled stirring solution of potassium carbazolide (3 equiv, 64 mg, 0.15 mmol) in 2 mL at –70 °C. The blue solution was allowed to stir for 5 h. The EPR spectrum of the crude mixture showed complete conversion of $CuBr_2$ to the $Cu^{II}(carbazolide)_3^-$ anion (Figure S4). The solution was then filtered through a PTFE syringe filter, and a THF solution of benzo-15-crown-5 (2 equiv, 26 mg, 0.1 mmol) in 1 mL THF was added at –70 °C. The mixture was allowed to stand overnight at –70 °C to give a deep blue suspension containing a deep blue precipitate. The precipitate was collected while cold atop a sintered glass frit and washed with cold Et_2O to yield $[K(benzo\text{-}15\text{-}crown\text{-}5)_2][Cu^{II}(carbazolide)_3]$ (30 mg, 26% yield). Crystals were grown by layering Et_2O onto the solution in THF at –70 °C. The blue solid was stored at -30 °C.

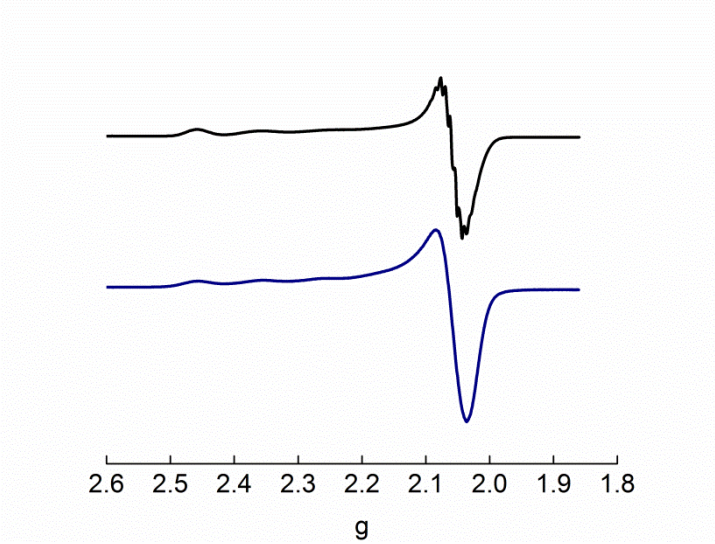

Figure S4: X-Band EPR spectra of [K(benzo-15-crown-5)$_2$][Cu^{II}(carbazolide)$_3$] in butyronitrile glass (black trace, 77 K) and in the solid-state (blue trace, 77 K).

V. Procedures for freeze-quench EPR studies

Stoichiometric reaction between [Li(MeCN)][Cu(carb)$_2$] and 2-bromo-4-phenylbutane under irradiation

[Li(MeCN)][Cu(carbazolide)$_2$] (4.4 mg, 0.01 mmol) and 2-bromo-4-phenylbutane (10 mg, 0.05 mmol) were added to a 4 mL vial. The mixture was dissolved in 0.3 mL butyronitrile, and the resulting solution was transferred to an EPR tube. The EPR tube was sealed and cooled to –78 °C. The EPR tube was irradiated in the Luzchem photoreactor (350 nm) while being introduced to a quartz Dewar filled with liquid nitrogen. Irradiation of the freezing solution proceeded for approximately 15 seconds.

Detection of EPR active [Li(CH$_3$CN)$_n$][Cu^{II}(carb)$_3$] in a catalytic reaction mixture

A 4 mL solution of the standard reaction mixture containing [Li(MeCN)$_n$][Cu(carbazolide)$_2$] (0.0067 mmol), lithium carbazolide (0.2 mmol), and alkyl bromide (0.13 mmol) was prepared in a 4 mL borosilicate glass vial according to the standard procedure using butyronitrile as the solvent. A portion of the resulting solution (300 μL) was transferred to an EPR tube. The tube was sealed and cooled to 0 °C, and irradiated with a 100-watt Hg lamp at 0 °C. Alternatively, an aliquot (0.1 mL) of the standard reaction mixture in acetonitrile in a 4 mL borosilicate vial that was irradiated for 1 h was transferred to a pre-cooled EPR tube containing butyronitrile (0.2 mL) under N_2. The EPR tube was briefly shaken and cooled to 77 K. Simulation parameters are as follows: g = [2.318, 2.058, 2.050]; H_{Strain} (MHz) = [120, 5, 5]; A_{Cu} (MHz) = [350 25 21] A_{3N} (MHz) = [50,35,35].

Generation and detection of EPR active [Li(CH$_3$CN)$_n$][Cu^{II}(carb)$_3$] via metallation

A pre-chilled solution of $CuBr_2$ (2.2 mg, 0.01 mmol) in 1 mL acetonitrile was added dropwise to a pre-chilled slurry of lithium carbazolide (5.3 mg, 0.03 mmol) in the glovebox. The deep blue solution was allowed to stir for 5 min before transferring an aliquot to a solution of butyronitrile in acetone/dry ice bath. The solution was then transferred to an EPR tube.

Detection of EPR active [Li(CH$_3$CN)$_n$][Cu^{II}(carb)$_3$] via oxidation of [Li(MeCN)][Cu(carb)$_2$]

[Li(MeCN)][Cu(carbazolide)$_2$] (10.0 mg, 0.023 mmol) and lithium carbazolide (8 mg, 0.046 mmol) were mixed in 200 μL of butyronitrile, added to an EPR tube, and frozen at 77 K. To this frozen layer was added a 200 μL solution of tris(4-bromophenyl)ammoniumyl hexachloroantimonate ("Magic Blue", 3.4 mg, 0.0042 mmol) in butyronitrile. The solutions were allowed to mix briefly (~5 s) in thawing butyronitrile and frozen again.

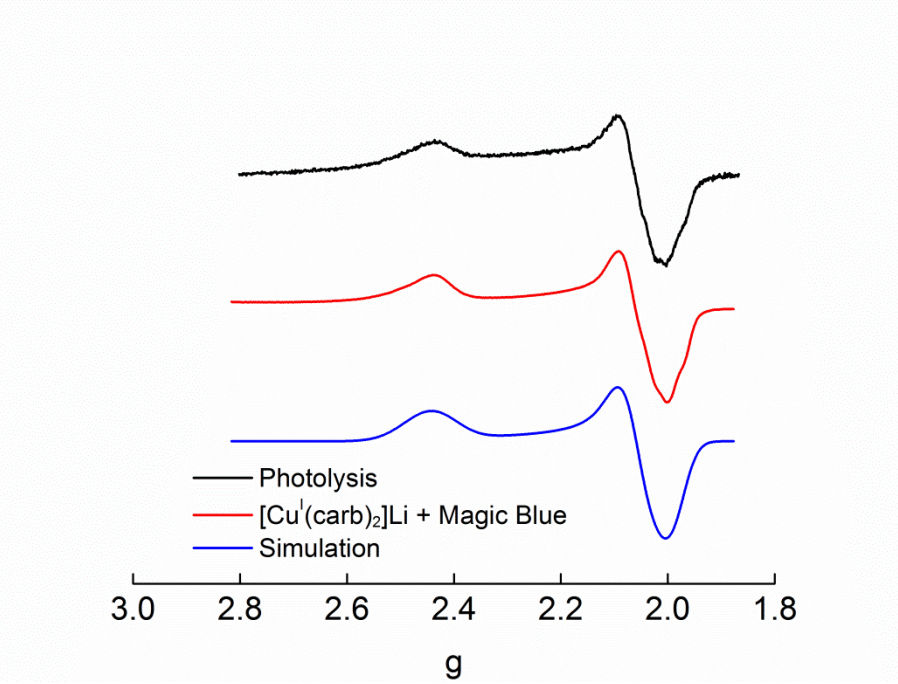

Figure S5: EPR spectra (9.4 GHz, 77 K). Black trace: mixture of $[Cu^{I}(carb)_2]Li$ and 2-bromo-4-phenylbutane (5 equiv) in freezing butyronitrile upon irradiation at 350 nm; red trace: mixture of $[Cu^{I}(carb)_2]Li$ and Magic Blue (0.2 equiv) in butyronitrile at –80 °C; blue trace: simulation of red trace. Simulation parameters: g = [2.445, 2.060, 1.994]; isotropic linewidth (Gaussian lineshape, FWHM = 10 mT). Coupling to one Cu nucleus was included with A = [75, 1, 1].

VI. Procedures for UV-vis studies

Molar absorptivity of $[Li(CH_3CN)_n][Cu^{II}(carb)_3]$ at 580 nm

A 20 mL vial was charged with lithium carbazolide (5.5 mg, 0.030 mmol) and a magnetic stir bar. Acetonitrile (9.0 mL) was added to the vial, and the solution was cooled to thawing acetonitrile temperature. A separate vial was charged with $CuBr_2$ (6.6 mg, 0.030 mmol) and acetonitrile (3.0 mL). 1 mL of the resulting green solution of $CuBr_2$ (0.010 mmol) was added dropwise to the thawing acetonitrile solution of lithium carbazolide. After completed addition, the deep blue solution was allowed to stir vigorously at thawing acetonitrile temperature for approximately 30 minutes. The solution was transferred into a prechilled 1 cm pathlength quartz cuvette. The cuvette was capped and quickly inserted into the -40 °C UV-vis sample holder. The average molar absorptivity at 580 nm was found to be 1100 M^{-1} cm^{-1}.

Table S4: Measured molar absorptivity (580 nm) of $[Li(CH_3CN)_n][Cu^{II}(carb)_3]$ at various concentrations.

Concentration (mM)	Absorbance	Molar Absorptivity (M^{-1} cm^{-1})
0.103	1.170	1140
0.100	1.092	1092
0.083	1.028	1233
0.050	0.608	1216

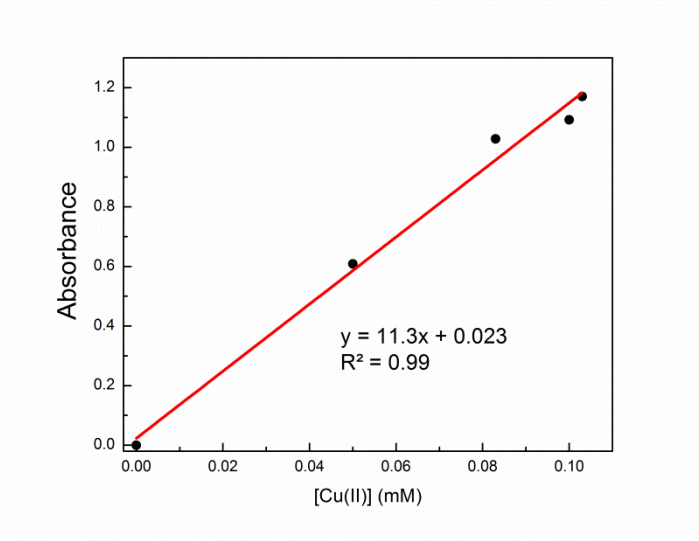

Figure S6: Absorbance at 580 nm as a function of concentration of Cu(II); path length = 1 cm.

Detection of $[Li(CH_3CN)_n][Cu^{II}(carb)_3]$ during catalysis

A 4 mL acetonitrile solution of the standard reaction mixture containing $[Li(MeCN)_n][Cu(carbazolide)_2]$ (2.9 mg, 0.0067 mmol), lithium carbazolide (34 mg, 0.19 mmol), and 2-bromo-4-phenylbutane (28 mg, 0.13 mmol) was prepared in a quartz cuvette with a stirbar. The reaction mixture was allowed to cool for 10 minutes in the dark at 0 °C in an ice bath. Then

the mixture was irradiated with a 100-watt Hg lamp while stirring, and UV-vis spectra were collected at 0 °C at various times after irradiation until the Cu(II) absorption at 580 nm was maximized.

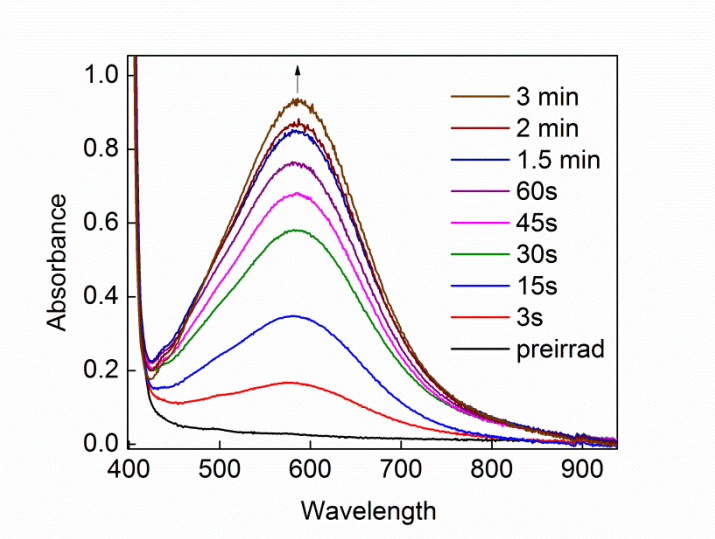

Figure S7: Appearance of Cu(II) absorption band at short irradiation times of reaction mixture.

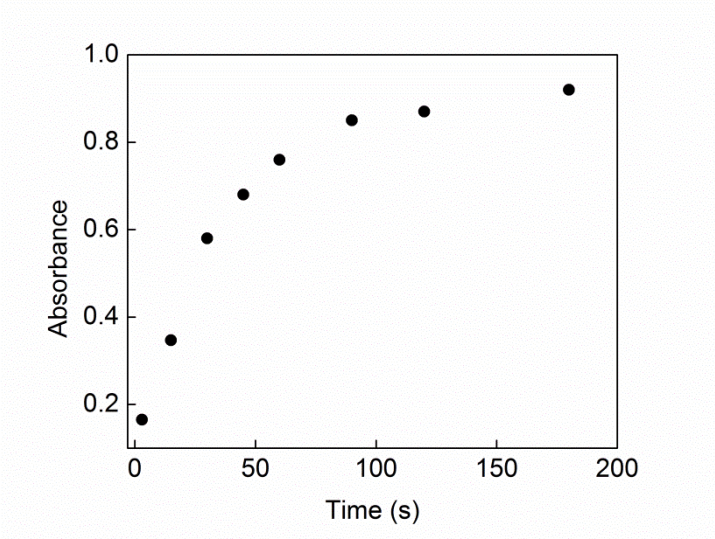

Figure S8: Absorbance at 580 nm at short irradiation times of reaction mixture.

Generation and detection of $[Li(CH_3CN)_n][Cu^{II}(carb)_3]$ via oxidation of $[Li(MeCN)][Cu(carb)_2]$

In a glovebox atmosphere, a 4 mL butyronitrile solution containing $[Li(MeCN)_n][Cu(carbazolide)_2]$ (0.037 mmol) and lithium carbazolide (0.074 mmol) was prepared in a quartz cuvette with a stirbar and sealed with a septum. Another solution containing tris(4-bromophenyl)ammoniumyl hexachloroantimonate ("Magic Blue", 0.012 mmol) was dissolved in 0.2 mL butyronitrile and taken up into a 1 mL Hamilton sample locked syringe, and the needle was pierced through a septum to prevent the introduction of air. The cuvette was

cooled to -80 °C in the UV-vis sample holder, and the syringe with Magic Blue was pierced through the cuvette septum. The sample lock was opened and the solution of Magic Blue was introduced into the mixture with vigorous stirring. The stirring was stopped and the sample was allowed to stabilize before a spectrum was acquired.

Molar absorptivity of [Li(MeCN)][Cu(carbazolide)$_2$] at 365 nm

A 1.9 mM solution of [Li(MeCN)][Cu(carbazolide)$_2$] was made by dissolving 4.2 mg (0.0095 mmol) in 5 mL acetonitrile, and this solution was used as a stock to generate lower concentration solutions of the complex. Each solution was pipetted into a 1 mm path length cuvette and absorption spectra were acquired at room temperature for each concentration. The molar absorptivity for [Li(MeCN)][Cu(carbazolide)$_2$] at 365 nm was found to be 4300 M^{-1} cm^{-1}.

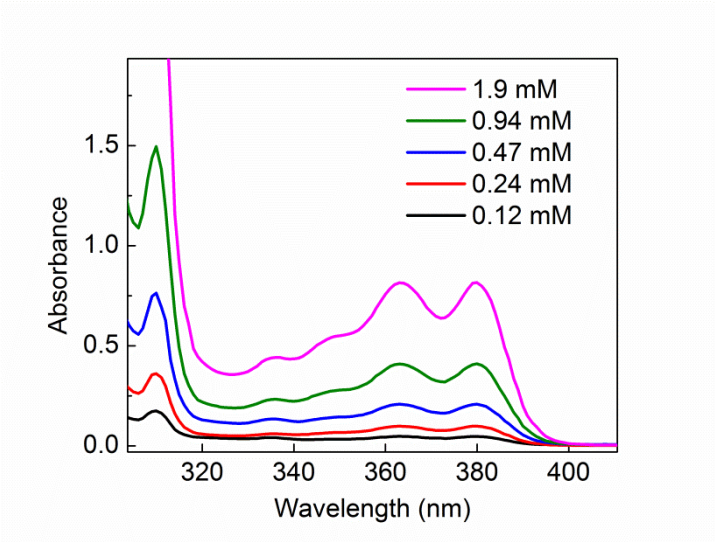

Figure S9: UV-vis spectra of [Li(MeCN)][Cu(carbazolide)$_2$] at various concentrations in CH_3CN at room temperature in 1 mm cuvette.

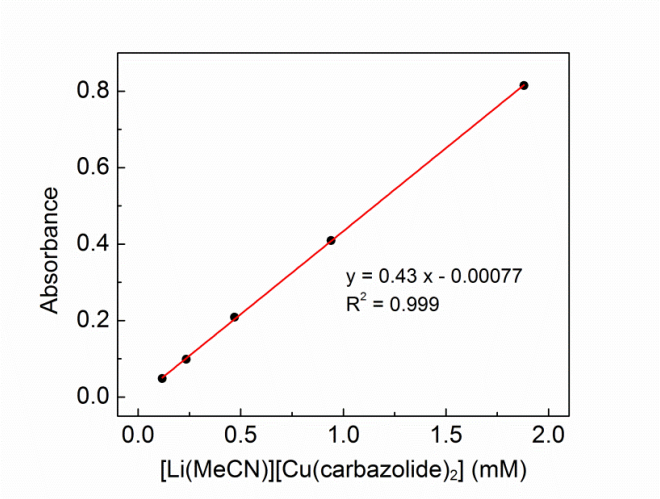

Figure S10: Absorbance at 365 nm as a function of [Li(MeCN)][Cu(carbazolide)$_2$] concentration; path length = 1 mm.

Molar absorptivity of lithium carbazolide at 365 nm

A 10 mM solution of lithium carbazolide was made, and this solution was used as a stock to generate lower concentration solutions of the complex. Each solution was pipetted into a 1 mm path length cuvette and absorption spectra were acquired at room temperature for each concentration. The molar absorptivity at 365 nm for concentrations of lithium carbazolide greater than 0.4 mM was found to be 2200 M^{-1} cm^{-1}.

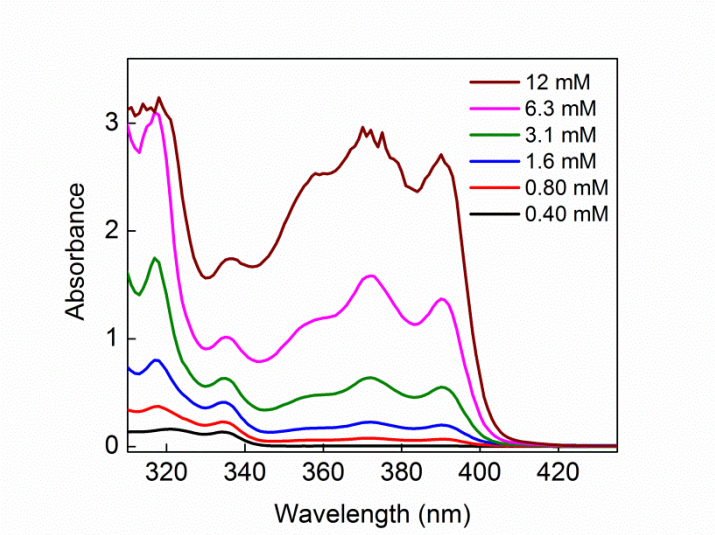

Figure S11: UV-vis spectra of lithium carbazolide at various concentrations in CH_3CN at room temperature in 1 mm cuvette.

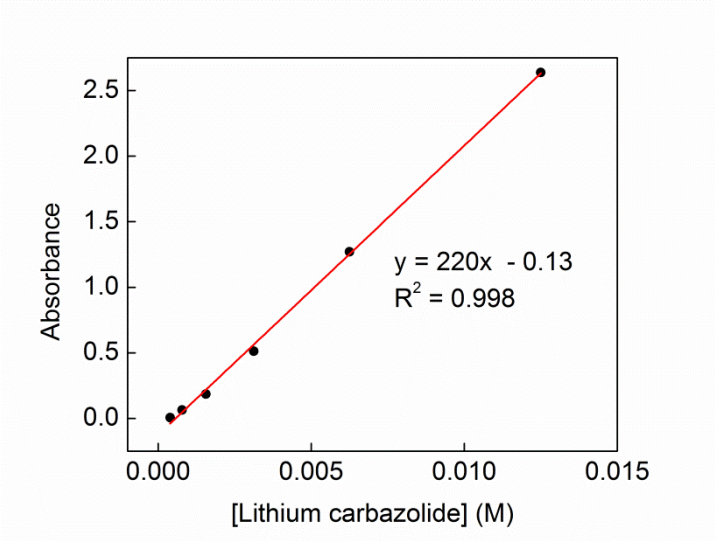

Figure S12: Absorbance at 365 nm as a function of lithium carbazolide concentration; path length = 1 mm.

VII. Procedures for DOSY analysis

Equimolar quantities of lithium carbazolide and 1,3,5-trimethoxybenzene (as an internal standard) were dissolved in 500 μL CD_3CN at concentrations ranging from 0.8 mM to 150 mM lithium carbazolide/1,3,5-trimethoxybenzene. A DOSY spectrum was acquired on a Varian 500 MHz spectrometer with a probe temperature of 25.0 °C, and the diffusion constants were calculated by an exponential fit for each of the four lithium carbazolide resonances in the ^{1}H NMR spectrum. Average hydrodynamic radii were calculated from each of the four diffusion constants using the Stokes-Einstein equation. The hydrodynamic radius for 1,3,5-trimethoxybenzene was similarly calculated as an average for both of its ^{1}H NMR resonances.

Table S5: Measured hydrodynamic radii and volumes.

[Lithium carbazolide] (mM)	Lithium carbazolide R_h (Å), average of 4	Lithium carbazolide vol. (Å^3)	1,3,5-trimethoxybenzene R_h (Å)	1,3,5-trimethoxybenzene vol. (Å^3)	MeCN R_h (Å)	MeCN vol. (Å^3)
0.8	3.07	121.2	3.03	116.5	1.61	17.5
2	3.10	124.8	2.96	108.6	1.58	16.5
4	3.52	157.5	3.06	118.8	1.68	19.9
8	3.66	205.4	2.95	107.5	1.62	17.8
49	4.61	410.4	3.21	138.5	1.73	21.7
98	4.77	454.6	3.26	145.1	1.79	24.0
150	4.81	466.1	3.3	150.5	1.76	22.8
carbazole (4.8 mM)	2.79	91.0	3.13	128.4	1.61	17.5

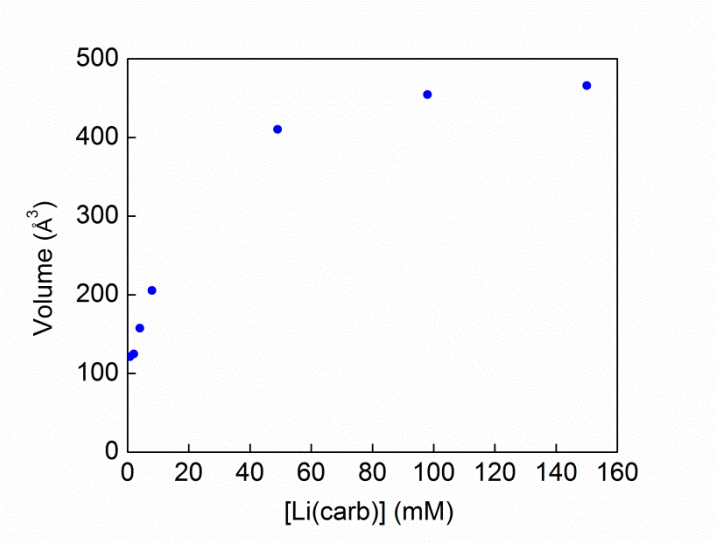

Figure S13: The hydrodynamic volume of lithium carbazolide increases as a function of increasing lithium carbazolide concentration.

VIII. Actinometric studies

Determination of light intensity

The Hatchard-Parker method was used to make a 0.006 M potassium ferrioxalate solution in 0.1 N H_2SO_4.[9] A 4 mL ferrioxalate solution in a quartz cuvette was then irradiated at 0 °C for 40 s in three separate runs using a 365 nm LED (Thorlabs, M365L2) and a focusing lens.

Sample photon flux calculation for 40 s photolysis:

$$I = \frac{AV_2V_3}{\varepsilon d \Phi_\lambda t V_1}$$

Where I is the intensity in einsteins/min, A is the absorbance (at 510 nm) of irradiated actinometer solution, V_2 is the volume (in L) of actinometer irradiated, V_3 is the volume (10 mL) of the volumetric flask used for the dilution of the irradiated aliquot, ε is the extinction coefficient of the ferrous 1,10-phenanthroline complex at 510 nm (1.11 x 10^4 L mol^{-1} cm^{-1}), d is the path length (in cm) of the cuvette used to measure the absorbance, Φ_λ is the quantum yield of ferrous production at 365 nm (1.21), t is the time of irradiation (in min), and V_1 is the volume (in mL) of irradiated actinometer solution withdrawn.

$$I = \frac{(0.19)(0.004\ L)(10\ mL)}{(1.11 \text{ x } 10^4\ M^{-1}cm^{-1})(1\ cm)(1.21)\left(\frac{40s}{60s/min}\right)(0.5\ mL)}$$

$$\boldsymbol{I = 1.7 \text{ x } 10^{-6}\ Einsteins/minute}$$

A photon flux of 1.7(5) x 10^{-6} Einsteins/minute was calculated by averaging all runs.

Determination of quantum yield for stoichiometric model reaction

A 4 mL acetonitrile solution of the standard reaction mixture containing [Li(MeCN)][Cu(carbazolide)$_2$] (0.0067 mmol), lithium carbazolide (0.2 mmol), and alkyl bromide (0.13 mmol) was prepared in a 1 cm path length quartz cuvette with a stirbar. The reaction mixture was allowed to cool to 0 °C with an internal cooling loop in a cuvette holder. Then, the mixture was irradiated with the 365 nm LED while stirring. After irradiation, the reaction mixture was diluted with diethyl ether and dodecane as an internal standard. An aliquot was filtered through a short pad of silica gel (ethyl acetate eluent) and the sample was injected for GC analysis. The quantum yield (Φ) was then determined by the following equation:

$$\Phi = \frac{moles\ of\ electrophile\ consumed}{Light\ intensity * time\ irradiated\ (min)}$$

The quantum yield was determined to be 0.099.

IX. Stern-Volmer quenching and determining quenching efficiency

Quenching of [Li(MeCN)][Cu(carbazolide)$_2$] with electrophile

[Li(MeCN)][Cu(carbazolide)$_2$] was diluted in acetonitrile to make a 0.00335 M solution. (3-bromobutyl)benzene was also diluted in acetonitrile to make 100, 200, 400, 600, 700, and 800 mM solutions. In 4 mL vials, a 250 μL aliquot of the solution containing [Li(MeCN)][Cu(carbazolide)$_2$] was mixed with a 250 μL aliquot of either acetonitrile or one of the solutions containing electrophile, such that the concentration of the copper catalyst in each solution was equal to the standard reaction concentration, 0.0017 M. The solutions were pipetted into cuvettes with a path length of 1 mm. The lifetime of a non-emissive excited state of [Li(MeCN)][Cu(carbazolide)$_2$] as a function of electrophile concentration was measured by transient absorbance spectroscopy (λ_{pump} = 355 nm, λ_{probe} = 580 nm) (Figure S13). The lifetime of the short-lived, emissive excited state of [Li(MeCN)][Cu(carbazolide)$_2$] was measured at the picosecond time scale using luminescence spectroscopy, and was found to be 590 ps (Figure S14). Data were analyzed using Matlab R2014A with the default curve fitting function. The rate of electron transfer was calculated to be 4.8 x 10^6 M^{-1} cm^{-1}.

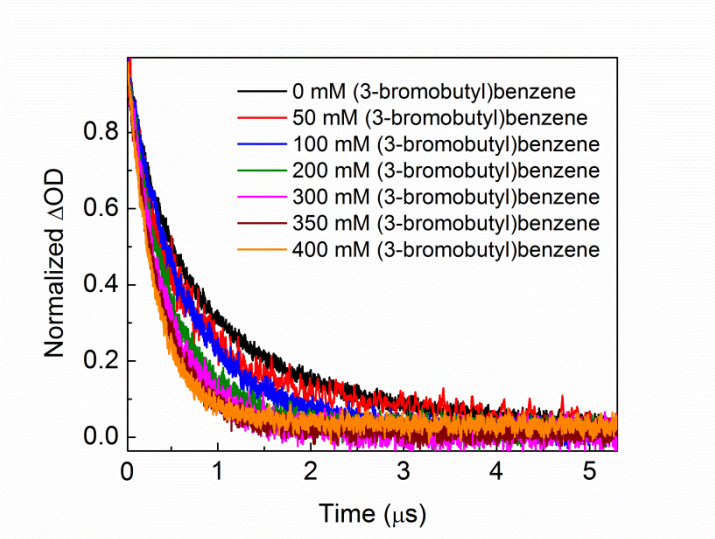

Figure S14: Transient absorbance decays for [Li(MeCN)][Cu(carbazolide)$_2$] with varying electrophile concentrations.

Table S6: Excited state lifetime of [Li(MeCN)][Cu(carbazolide)$_2$] as a function of electrophile concentration.

[(3-bromobutyl)benzene] (mM)	Lifetime (ns)
0	910
50	760
100	660
200	481
300	410
350	370
400	320

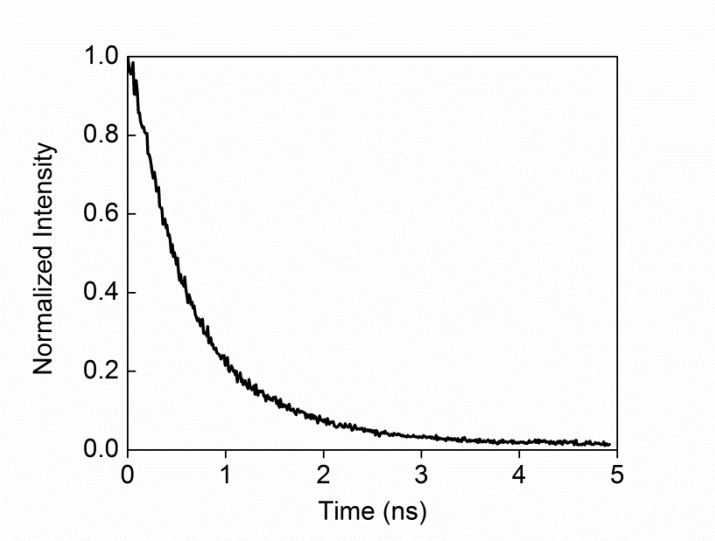

Figure S15: Luminescence decay of the emissive excited state of **1**.

Quenching of lithium carbazolide with electrophile

Lithium carbazolide (86.6 mg, 0.5 mmol) was diluted in a 10 mL volumetric flask with acetonitrile to make 10 mL of a 0.05 M solution (the concentration in the catalytic reactions). In four other volumetric flasks, the same amount of lithium carbazolide was weighed out, but only ~5 mL of acetonitrile was added. Then, (3-bromobutyl)benzene was added to the lithium carbazolide solutions *via* syringe to make 50, 100, 200, or 400 mM solutions of electrophile in 10 mL acetonitrile, and acetonitrile was added to the mark. For each run, one of these solutions was syringed into the Harrick flow cell described above (100 μm path length) until there were no gas bubbles, and flowed through with a syringe pump while fluorescence measurements were being collected. After each run, the flow cell was cleaned and dried under vacuum, and the next

solution was syringed into the cell. The rate of electron transfer was calculated to be 4.9 x 10^8 M^{-1} s^{-1}.

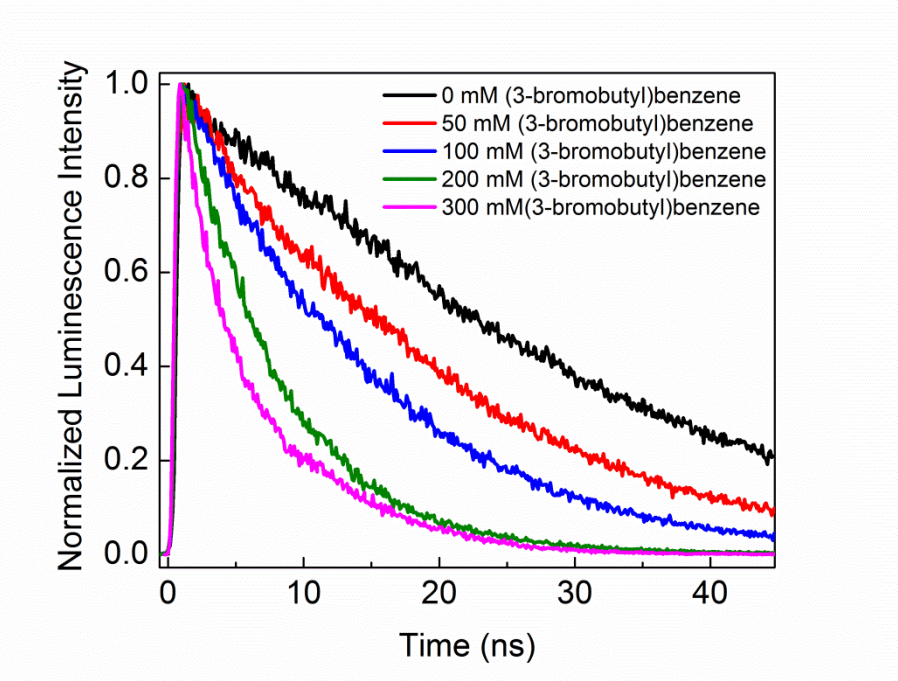

Figure S16: Luminescence decays for lithium carbazolide with varying electrophile concentrations.

Table S7: Excited state lifetime of lithium carbazolide as a function of electrophile concentration.

[(3-bromobutyl)benzene] (mM)	Lifetime (ns)
0	31
50	19.4
100	14
200	7.1
300	5.8

Self-quenching of [Li(MeCN)][Cu(carbazolide)$_2$]

[Li(MeCN)][Cu(carbazolide)$_2$] (4.2 mg, 0.0094 mmol) was diluted in 5 mL acetonitrile to make a 1.9 mM stock solution. This solution was serially diluted to make 0.94, 0.47, and 0.12 mM solutions. The solutions were pipetted into cuvettes with a path length of 1 mm. The excited state lifetime of [Li(MeCN)][Cu(carbazolide)$_2$] as a function of electrophile concentration was measured by transient absorbance spectroscopy (λ_{pump} = 355 nm, λ_{probe} = 580 nm). Logarithmically compressed data were analyzed using Matlab R2014A with the default curve fitting function. The rate of self-quenching was found to be 2.9 x 10^8 M^{-1} s^{-1}.

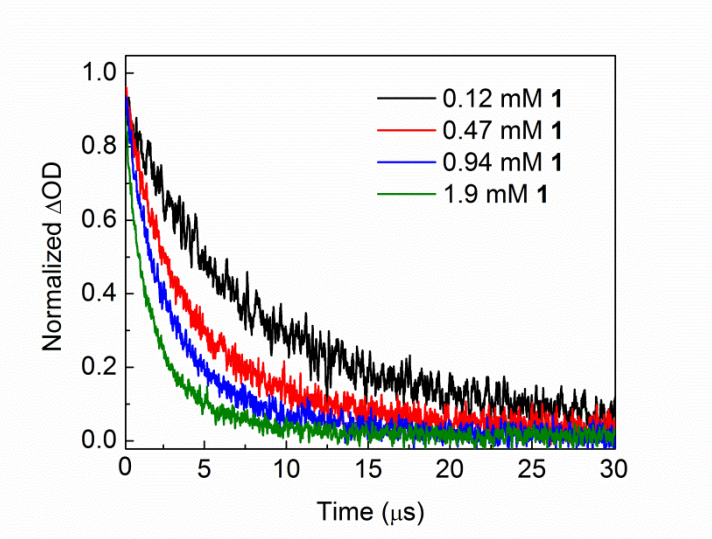

Figure S17: Transient absorbance decays for [Li(MeCN)][Cu(carbazolide)$_2$] at varying concentrations.

Table S8: Excited state lifetime of [Li(MeCN)][Cu(carbazolide)$_2$] as a function of concentration.

[[Li(MeCN)][Cu(carbazolide)$_2$] (mM)	**Lifetime (μs)**
0.12	7.5
0.47	3.6
0.94	2.6
1.9	1.51

Self-quenching of lithium carbazolide

Lithium carbazolide (43.3 mg, 0.25 mmol) was diluted in 5 mL of acetonitrile to make a 0.05 M solution (the concentration in the catalytic reactions). This solution was serially diluted to make 4.3, 2.2, 1.1, and 0.50 mM solutions. The solutions were pipetted into cuvettes with a path length of 1 mm. The excited state lifetime of lithium carbazolide as a function of electrophile concentration was measured by transient absorbance spectroscopy (λ_{pump} = 355 nm, λ_{probe} = 580 nm). Data were analyzed using Matlab R2014A with the default curve fitting function. The rate of self-quenching was found to be 2.0 x 10^7 M^{-1} s^{-1}. It is important to note that in the presence of electrophile quencher, this long-lived, non-emissive excited state was not observed, and S.E.T. seemed to proceed from the fluorescent state at a rate faster than that of intersystem crossing.

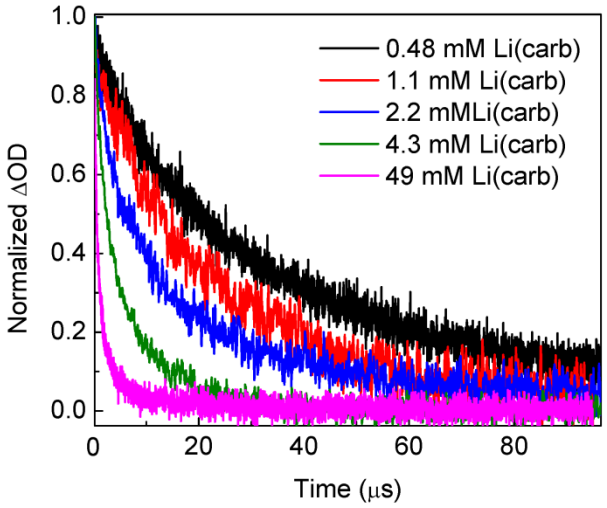

Figure S18: Transient absorbance decays for lithium carbazolide at varying concentrations.

Table S9: Excited state lifetime of [Li(MeCN)][Cu(carbazolide)$_2$] as a function of concentration

[Li(carb)] (mM)	Lifetime (μs)
0.5	33
1.1	22
2.2	14
4.3	5.8
49	1.0

Quenching efficiency of lithium carbazolide

The quenching fraction (Q) can be defined as the ratio of the rate at which the excited state photocatalyst (lithium carbazolide) is quenched productively (by electrophile) to the sum of the rates of all the other relaxation processes which are available to the excited state. In the case of lithium carbazolide, in addition to being quenched, the excited state can luminesce and also self-quench (after intersystem crossing to a lower-energy state; there is no evidence of self-quenching from the shorter-lived, emissive state). However, since the rate of self-quenching is only measured in the absence of electrophile, it is unclear what role self-quenching plays is in the presence of electrophile. Thus, we can only estimate an upper limit for the quenching fraction.

$$Q \leq \frac{k_q * [electrophile]}{\frac{1}{\tau_{0,Li}} + k_q * [electrophile]}$$

$$\leq \frac{(4.9 \text{ x } 10^8\ M^{-1}s^{-1})(0.0325\ M)}{\frac{1}{3.1 \text{ x } 10^{-8}s} + (4.9 \text{ x } 10^8\ M^{-1}s^{-1})(0.0325\ M)} \leq \mathbf{0.33}$$

This value for the quenching fraction implies that 33% of all lithium carbazolide excited states generated are quenched by electrophile. The remainder may be self-quenched or quenched by other species in solution.

The chain length is the ratio of the quantum yield to the quenching fraction, and a lower limit can be calculated:

$$Chain\ length \geq \frac{\Phi}{Q} \geq \frac{0.099}{0.33} \geq 0.30$$

This low value for chain length may be due to unproductive back electron transfer. In principle, the true chain length could be higher than 0.30 if, for example, Q is less than 0.33 due to self-quenching effects that we are unable to measure. Auto-quenching was observed for the excited state of $[Cu^{II}(carb)_3]Li$ with a rate constant of $5 \times 10^7\ M^{-1}\ s^{-1}$ from the long-lived, non-emissive state. However, this state is not accessible in the presence of electrophile, possibly because the rate of quenching is greater than the rate of intersystem crossing. Thus, the auto-quenching rate does not apply to a solution in which the electrophile is present. On the basis of our flash-quench analysis, we have calculated the upper limit for the quenching fraction to be 0.33.

X. Reactivity of $[Li(CH_3CN)_n][Cu^{II}(carb)_3]$

Decomposition of $[Li(CH_3CN)_n][Cu^{II}(carb)_3]$

A freshly prepared acetonitrile solution of $Li[Cu^{II}(carb)_3]$ in dry-ice/acetone bath was allowed to warm to room temperature overnight. The mixture was then concentrated in vacuo and the residue was loaded on a 20 cm x 20 cm Merck TLC plate. Two of many UV-active bands after developing the TLC in hexanes were identified as the commercially available 9,9-bicarbazyl and 3,3'-bicarbazole.

Decomposition of $[Li(CH_3CN)_n][Cu^{II}(carb)_3]$ in the presence of TEMPO–H

A freshly prepared solution of $Li[Cu^{II}(carb)_3]$ was prepared in thawing MeCN. A cold solution of 2,2,6,6-tetramethylpiperidin-1-ol [10] (TEMPO–H, 1 equiv) in MeCN was added to the cold solution of $Li[Cu^{II}(carb)_3]$, and the mixture was allowed to stir in thawing MeCN temperature for 30 min. A portion of the reaction mixture was transferred to an EPR tube and diluted with butyronitrile for X-band EPR measurement at 77 K. The only EPR active signal was that of 2,2,6,6-Tetramethylpiperidine 1-oxyl, and signals corresponding to a Cu^{II} species were absent. The analogous reaction conducted in CD_3CN at –45 °C shows the appearance of $[Cu^{I}(carb)_2]^-$ signal by ^1H NMR spectroscopy, consistent with the delivery of an H atom.

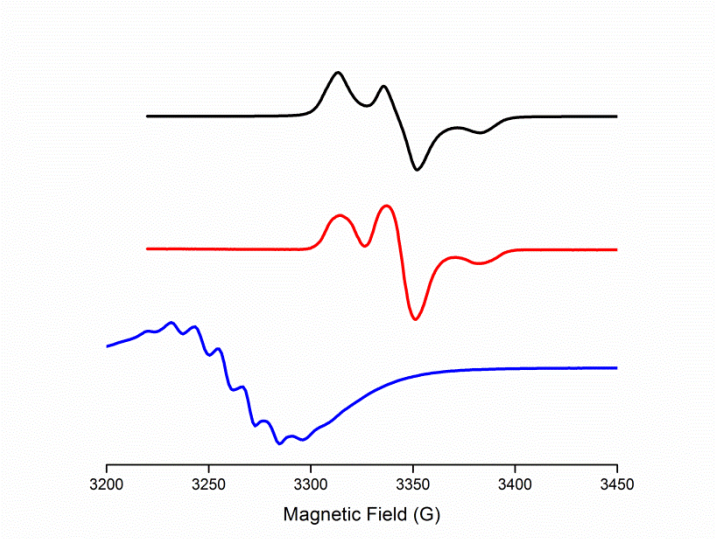

Figure S19: EPR spectra (9.4 GHz, 77 K, butyronitrile) of freshly made $Li[Cu^{II}(carb)_3]$ (blue trace), reaction of $Li[Cu^{II}(carb)_3]$ with TEMPO–H (red trace), and TEMPO (black).

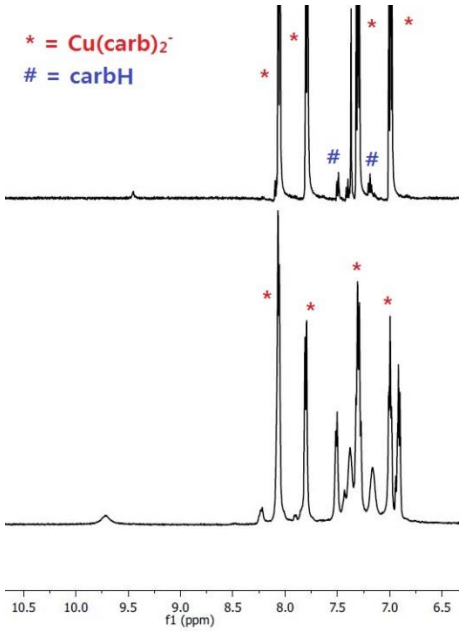

Figure S20: ^{1}H NMR spectra (500 MHz, -40 °C, CD_3CN) of a mixture of carbH and $[Li(CH_3CN)][Cu^{I}(carb)_2]$ (top) and of a mixture of $[Li(CH_3CN)_n][Cu^{II}(carb)_3]$ and TEMPOH (bottom).

XI. Computational methods

General considerations. The Orca 3.0.1 program was used for all calculations.[11] All optimizations and energy calculations were conducted with tight convergence criteria using the M06-l functional[12] and def2-TZVP basis set.[13] Open- and closed-shell species were modeled within the unrestricted and restricted Kohn-Sham formalisms, respectively. All geometry optimizations were conducted without symmetry constraints using gradient methods. Ground state geometries were verified as true minima by the absence of imaginary frequencies. All energies reported are Gibbs free energies at 298.15 K and include translational, rotational, vibrational, and solvation energy contributions. Solvation was treated with the conductor-like screening model, using default parameters for acetonitrile in all cases.[14] For $[Cu^{II}(carb)_3]^-$, the Loewdin spin density shown in Figure 11 was derived from a constrained optimization where the N-Cu-N angles and the C(1)-C(9a)-N-Cu dihedrals along each carbazole were constrained to match that of the experimentally determined solid-state crystal structure. The energy was derived from an unconstrained optimization. Time-dependent DFT calculations were performed using the M06l functional within the Tamm–Dancoff approximation employing the def2-TZVP basis set. The 50 lowest-lying excited states were calculated, based on the same constrained optimized geometry used for the spin density calculation. Solvation was treated with the conductor-like screening model, using values of $\varepsilon = 20$ and $\eta = 1.38$ for butyronitrile.

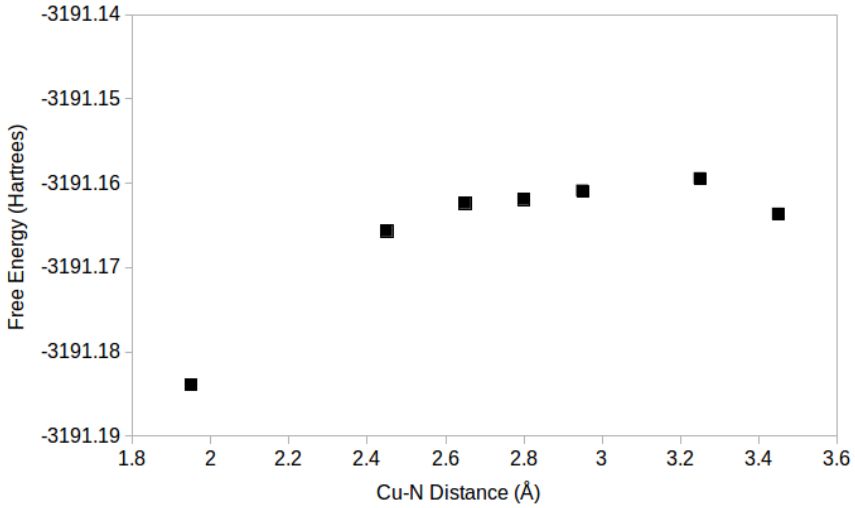

Figure S21: Relaxed surface scan for the reaction between $[Cu^{I}(carb)_2]^-$ and carb radical. Due to the shallow nature of the potential energy surface, a precise transition state could not be located.

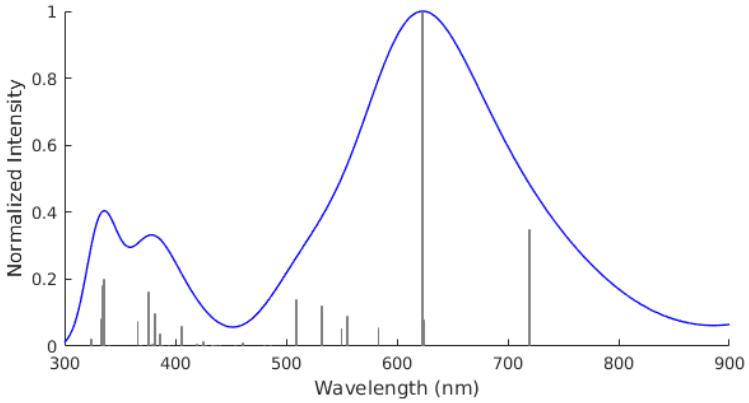

Figure 22: Absorbance spectrum of $[Cu^{II}(carb)_3]^-$ calculated by TD-DFT.

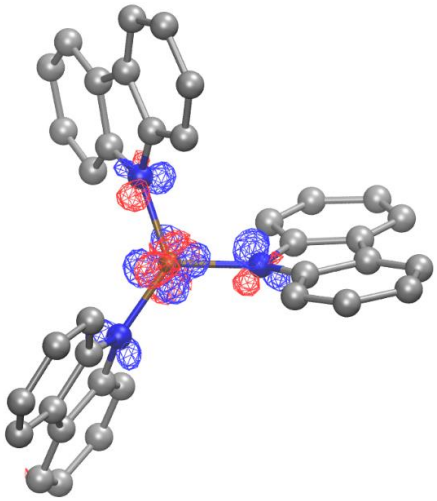

Figure 23: Difference density plot for the most intense calculated absorption band of $[Cu^{II}(carb)_3]^-$ at 623 nm. The donor orbital is shown in red, and the acceptor orbital is shown in blue.

Table S10: Free Energies of computed molecules

Compound	Gibbs Free Energy (Hartrees)
$[Cu^{I}(carb)_2]^-$	-2674.3593
$Cu^{II}(carb)_2$	-2674.2012
$[Cu^{II}(carb)_3]^-$	-3191.1839
$[Cu^{II}(carb)_2(^{i}Pr)]^-$	-2792.7926
$[carb]^-$	-516.9644
$(carb)\cdot$	-516.8096
$(^{i}Pr)\cdot$	-118.4381

XII. Characterization data for new coupling products

9-(hept-6-en-2-yl)-9*H*-carbazole:

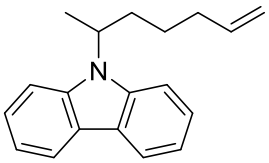

Following the general coupling procedure for 6-bromohept-1-ene, the title compound can be obtained after column chromatography (hexanes →1% ethyl acetate/hexanes) as a colorless oil. A typical run produces 10% of the coupling product according to calibrated GC analysis.

^{1}H NMR (300 MHz, Chloroform-*d*): δ 8.11 (d, J = 7.7 Hz, 2H), 7.65–7.34 (m, 4H), 7.20 (d, J = 7.6 Hz, 2H), 5.86–5.56 (m, 1H), 5.02–4.85 (m, 2H), 4.83–4.71 (m, 1H), 2.38–2.25 (m, 1H), 2.03–1.92 (m, 3H), 1.68 (d, J = 7.0 Hz, 3H), 1.49–1.29 (m, 1H), 1.25–1.13 (m, 1H).
^{13}C NMR (101 MHz, Benzene-d_6): δ 139.87, 138.14, 125.38, 123.55, 120.48, 118.76, 114.51, 110.00, 50.88, 34.00, 33.29, 25.97, 18.83.
MS (EI) m/z (M^+) calc for $C_{19}H_{21}N$: 263, found: 263.
FT-IR (film): 2931, 1640, 1625, 1594, 1482, 1451, 1331, 1316, 1223, 1157, 746, 721 cm^{-1}

9-((2-methylcyclopentyl)methyl)-9H-carbazole:

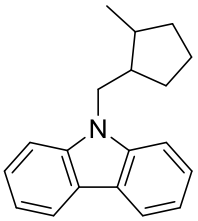

Following the general coupling procedure for 6-bromohept-1-ene, the title compound can be obtained as the mixture of diastereomers after column chromatography (hexanes →1% ethyl acetate/hexanes) as a colorless solid. A typical run produces 60% of the coupling product according to calibrated GC analysis. NMR resonances of the major diastereomer are as follows.

^{1}H NMR (400 MHz, Chloroform-*d*): δ 8.13 (d, J = 7.7 Hz, 2H), 7.54–7.38 (m, 4H), 7.27–7.21 (m, 2H), 4.40 (dd, J = 14.6, 4.6 Hz, 1H), 4.20 (dd, J = 14.6, 10.9 Hz, 1H), 2.74–2.45 (m, 1H), 2.28–2.22 (m, 1H), 1.96–1.72 (m, 2H), 1.53–1.38 (m, 4H), 1.15 (d, J = 7.1 Hz, 3H).
^{13}C NMR (126 MHz, Chloroform-*d*): δ 140.64, 125.48, 122.85, 120.31, 118.64, 108.88, 43.91, 42.94, 36.06, 33.19, 28.85, 22.53, 15.48.
FT-IR (film): 2954, 2870, 1597, 1484, 1461, 1452, 1326, 1218, 1153, 748, 722 cm^{-1}
MS (EI) m/z (M^+) calc for $C_{19}H_{21}N$: 263, found: 263.

^{1}H NMR resonances were assigned for major and minor diastereomers based on COSY data. Stereochemistry of the major diastereomer was assigned based on NOESY analysis.

9-((2-methylcyclopentyl)methyl-*d*)-9H-carbazole:

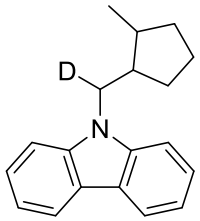

Following general coupling procedure with (E)-6-bromohept-1-ene-1-*d*, the title compound can be obtained as the mixture of diastereomers after column chromatography (hexanes →1% ethyl acetate/hexanes) as colorless solid. A typical run produces 60% of the coupling product according to calibrated GC analysis. NMR resonances of the major diastereomer are as follows.

^{1}H NMR (400 MHz, Benzene-d_6): δ 8.10-8.06 (m, 2H), 7.41-7.45 (m, 2H), 7.28-7.23 (m, 4H), 3.92-3.86 (m, 0.5H) 3.77-3.67 (m, 0.5H) 2.29-2.21 (m, 1H) 1.88-1.78 (m, 1H) 1.58-1.49 (m, 2H) 1.28-1.11 (m, 4H) 0.81 (d, J = 7.1 Hz, 3H)
^{13}C NMR (126 MHz, Benzene-d_6): δ 141.11, 125.83, 123.57, 120.82, 119.19, 109.27, 43.56 (t, J = 20.4 Hz), 42.99, 36.18, 33.31, 28.94, 22.74, 15.38.
^{2}H NMR (61 MHz, Benzene): δ 3.86, 3.70.
MS (EI) m/z (M^+) calc for $C_{19}H_{20}DN$: 264, found: 264.

XIII. ^{1}H, ^{2}H, and ^{13}C NMR spectra of new compounds

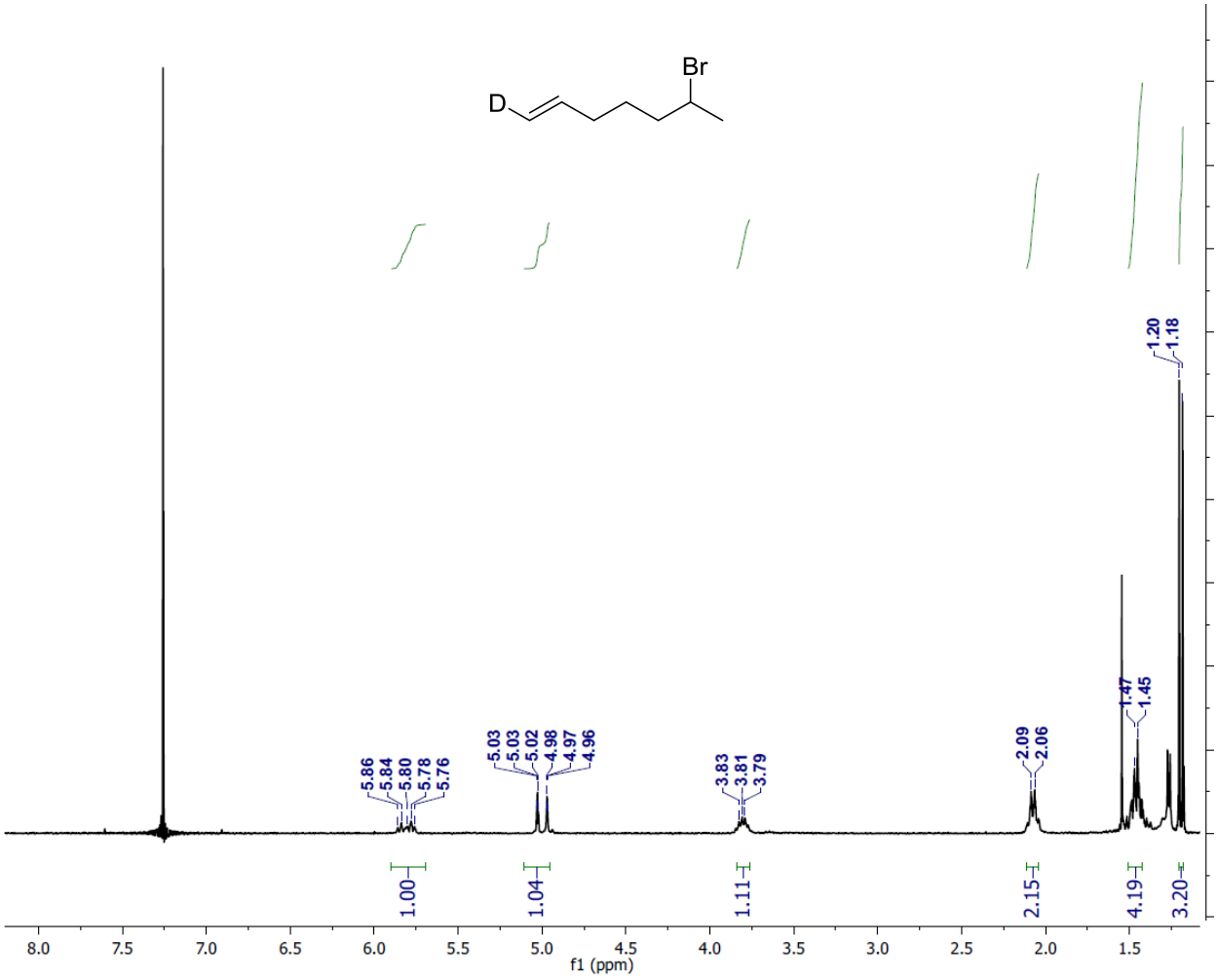

Figure S24: ^{1}H NMR spectrum of (E)-6-bromohept-1-ene-1-d ($CDCl_3$, 300 MHz, rt).

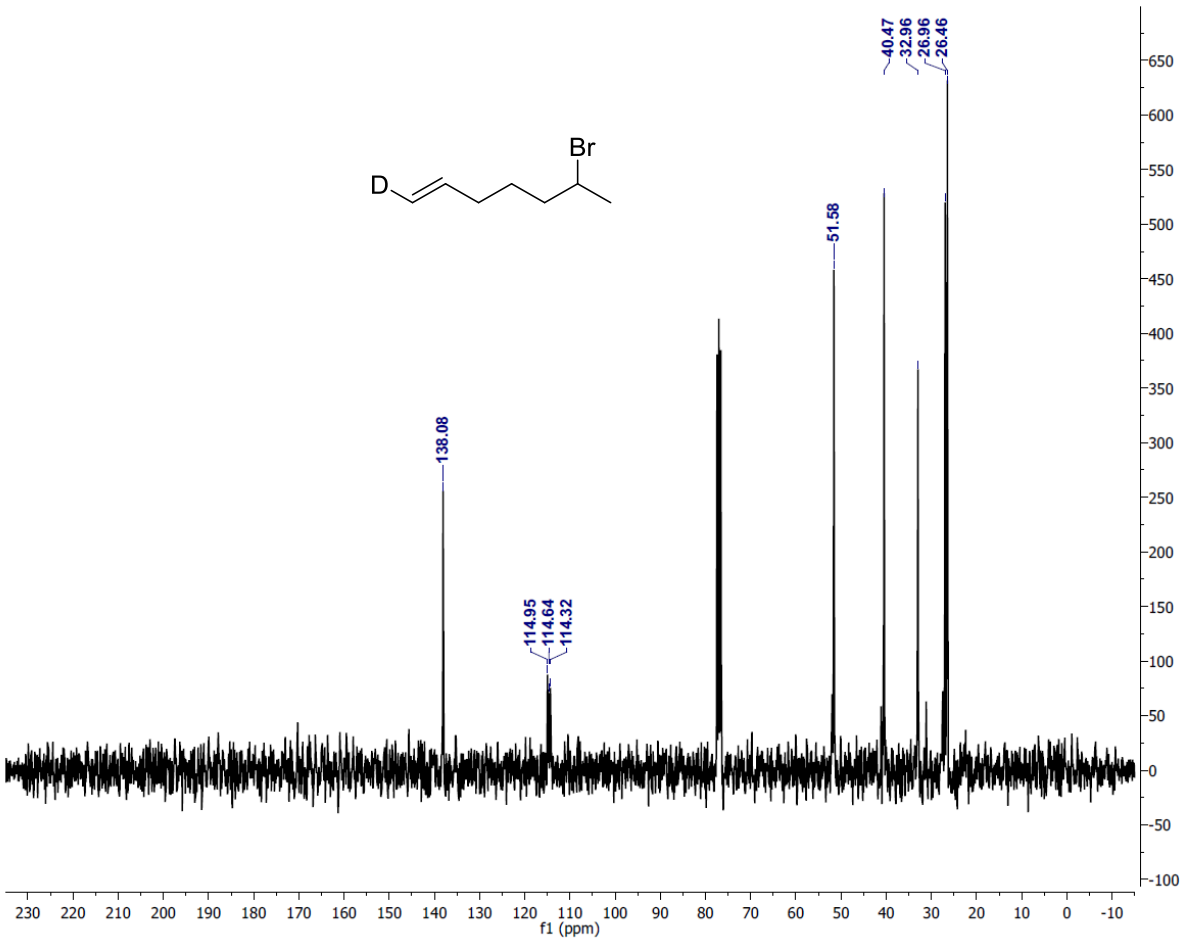

Figure S25: $^{13}C\{^{1}H\}$ NMR spectrum of (E)-6-bromohept-1-ene-1-d ($CDCl_3$, 75 MHz, rt).

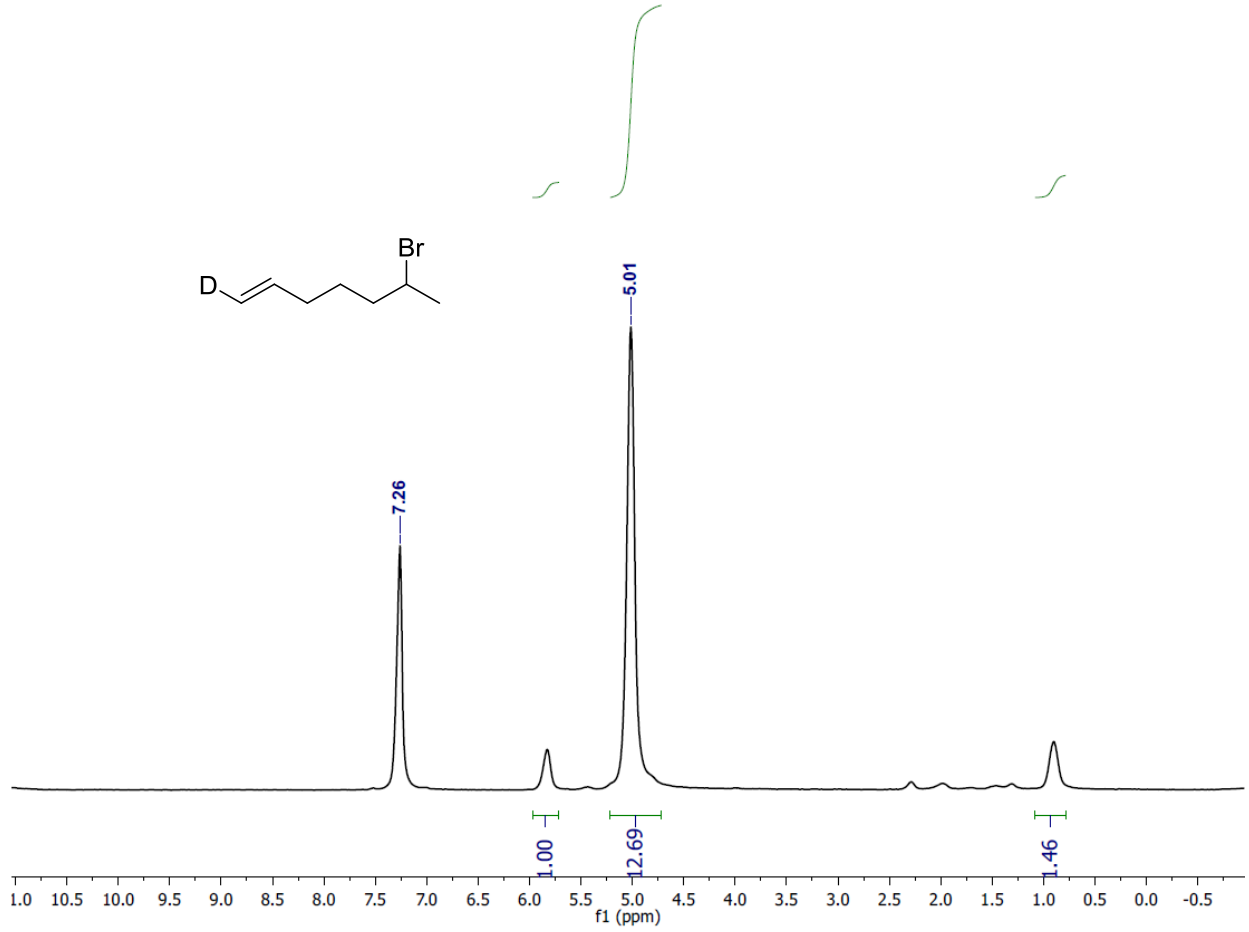

Figure S26: ^{2}H NMR spectrum of (E)-6-bromohept-1-ene-1-d ($CHCl_3$, 61 MHz, rt).

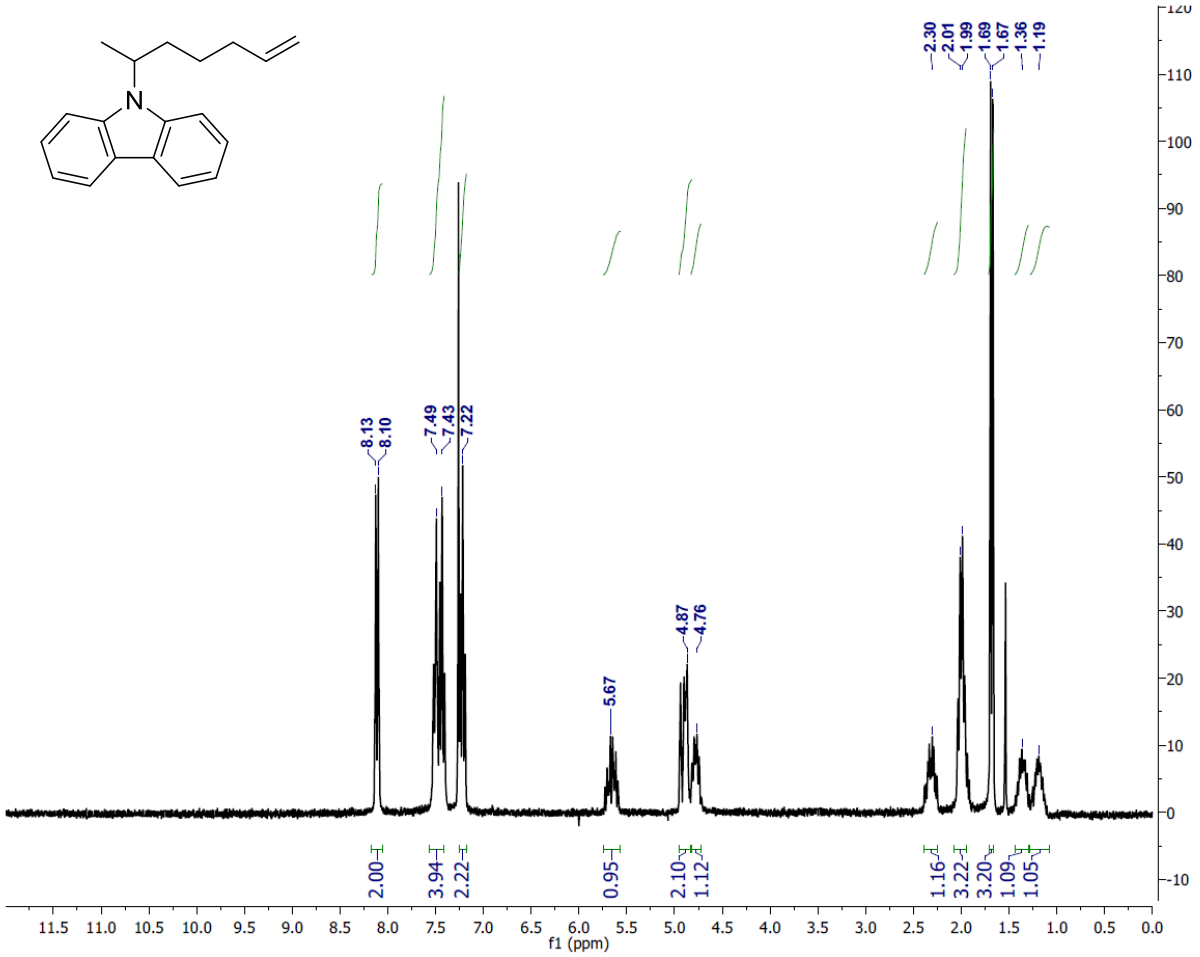

Figure S27: ^{1}H NMR spectrum of 9-(hept-6-en-2-yl)-9H-carbazole ($CDCl_3$, 300 MHz, rt).

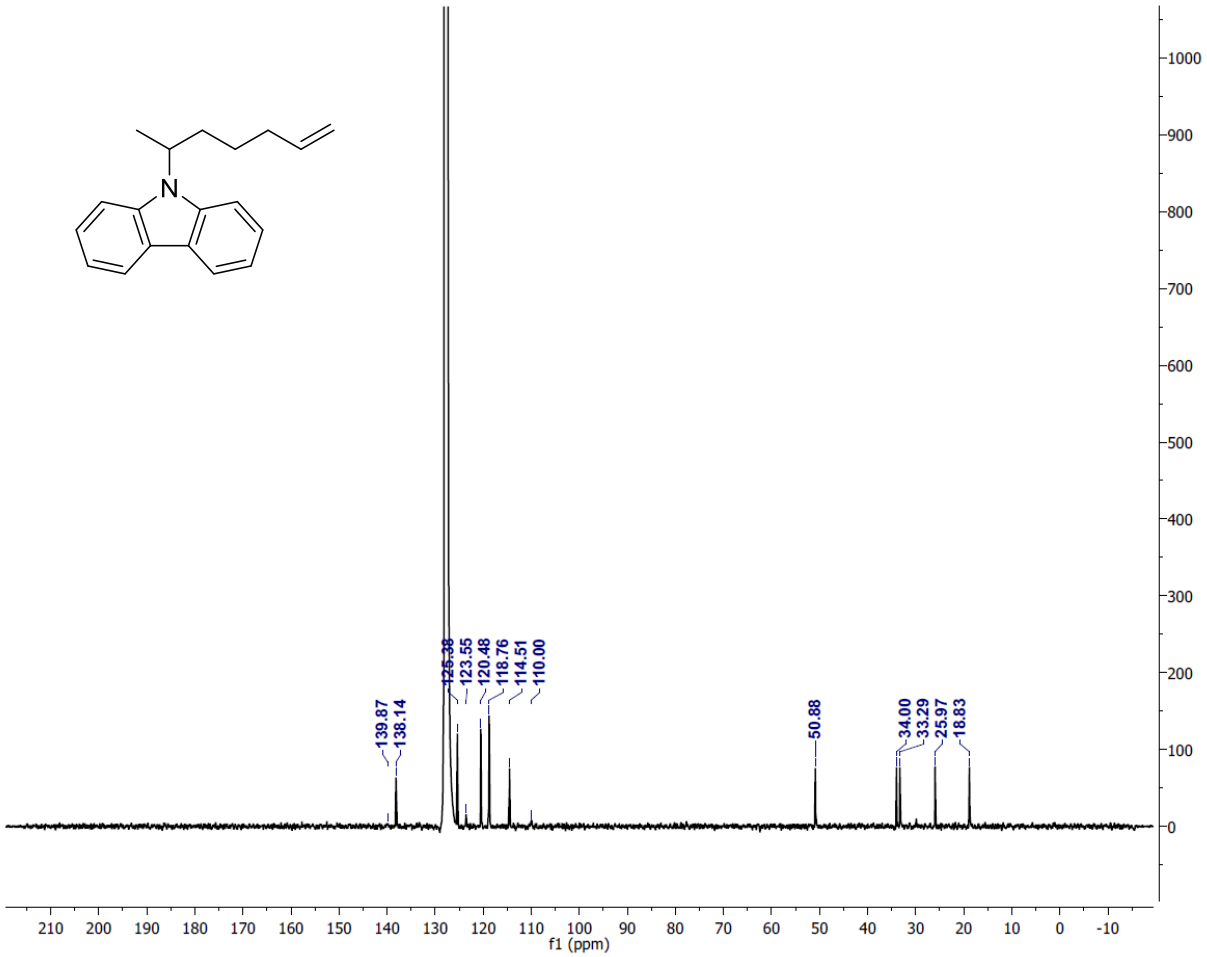

Figure S28: $^{13}C\{^{1}H\}$ NMR spectrum of 9-((2-methylcyclopentyl)methyl-d)-9H-carbazole (C_6D_6, 126 MHz, rt).

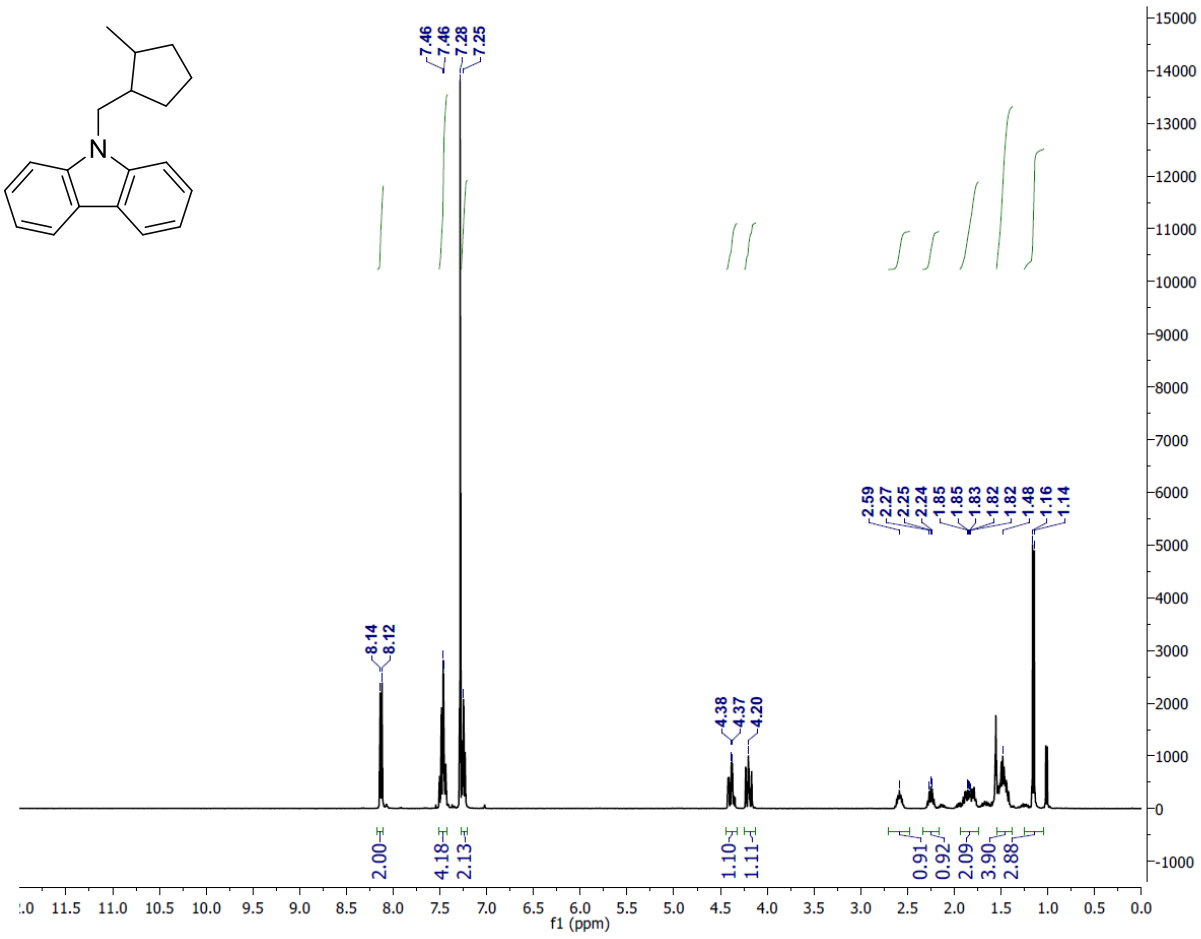

Figure S29: ^{1}H NMR spectrum of 9-((2-methylcyclopentyl)methyl)-9H-carbazole ($CDCl_3$, 400 MHz, rt).

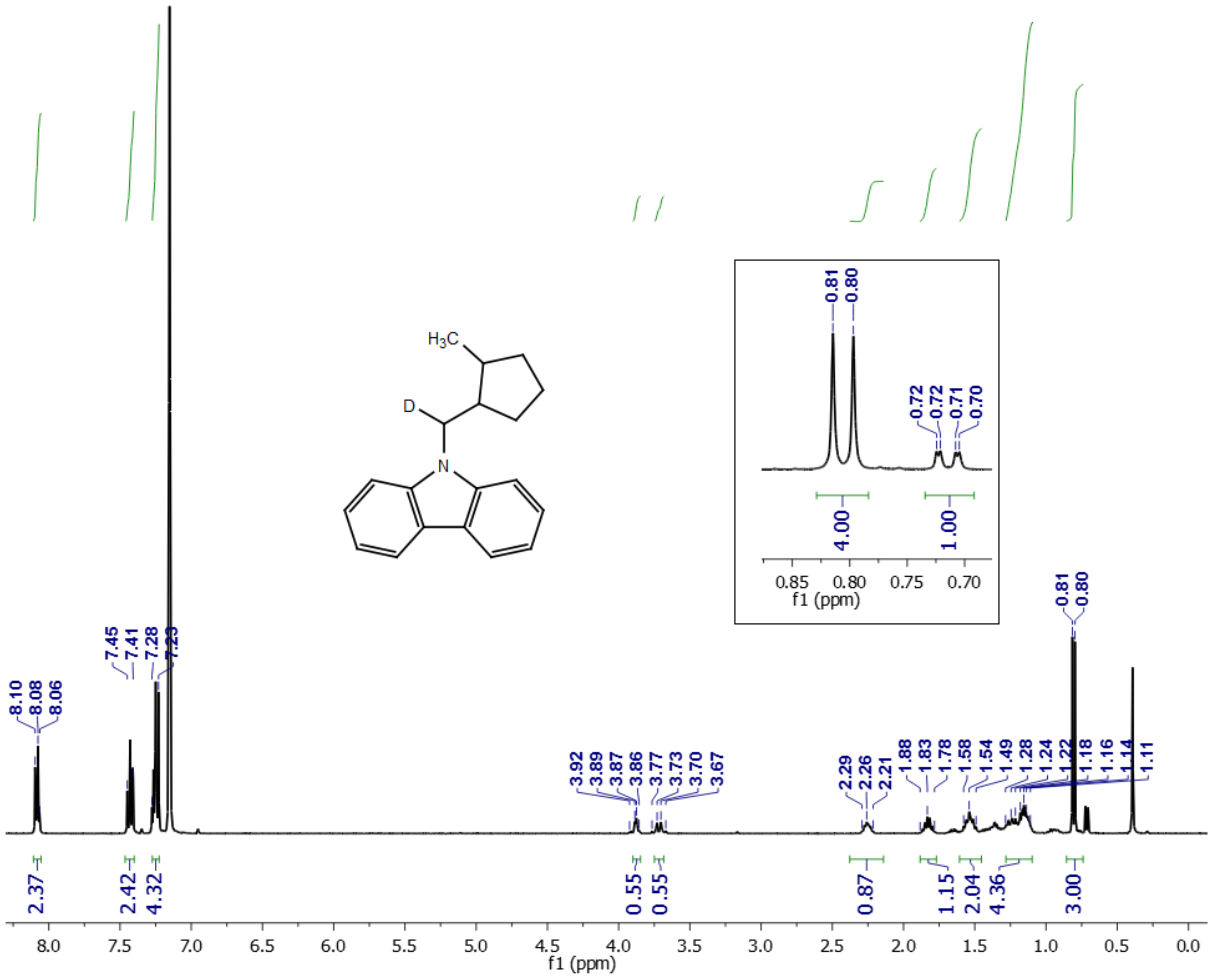

Figure S30: ^{1}H NMR spectrum of 9-((2-methylcyclopentyl)methyl-d)-9H-carbazole (C_6H_6, 400 MHz, rt).

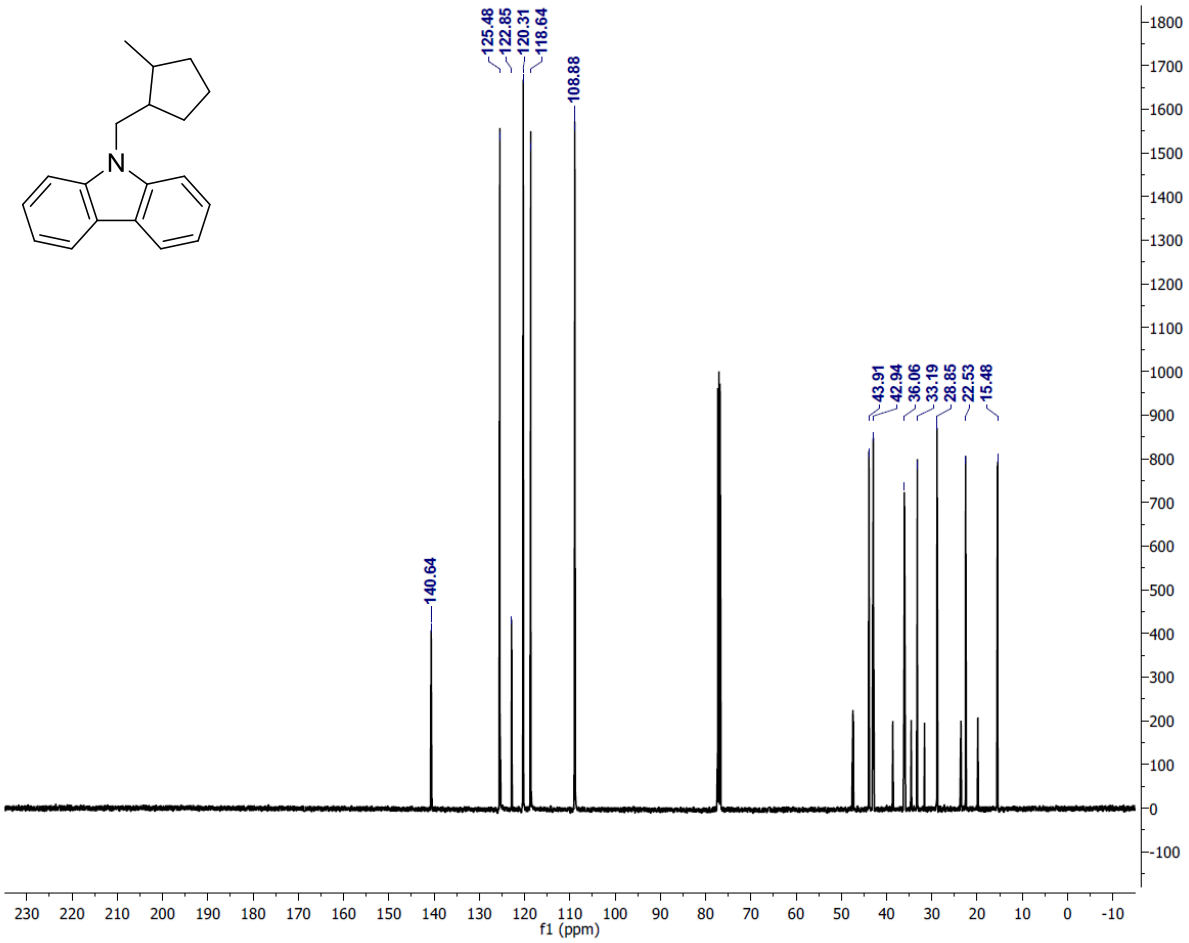

Figure S31: $^{13}C\{^{1}H\}$ NMR spectrum of 9-((2-methylcyclopentyl)methyl-d)-9H-carbazole (C_6D_6, 126 MHz, rt).

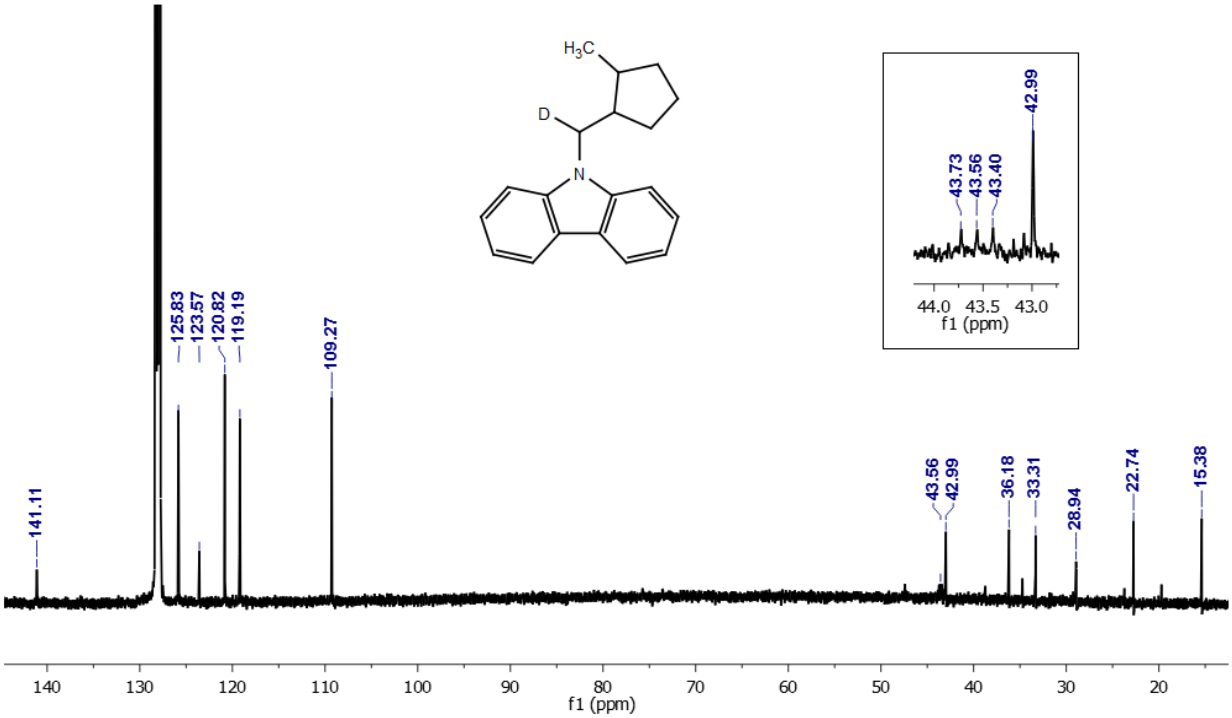

Figure S32: $^{13}C\{^{1}H\}$ NMR spectrum of 9-((2-methylcyclopentyl)methyl-d)-9H-carbazole (C_6D_6, 126 MHz, rt).

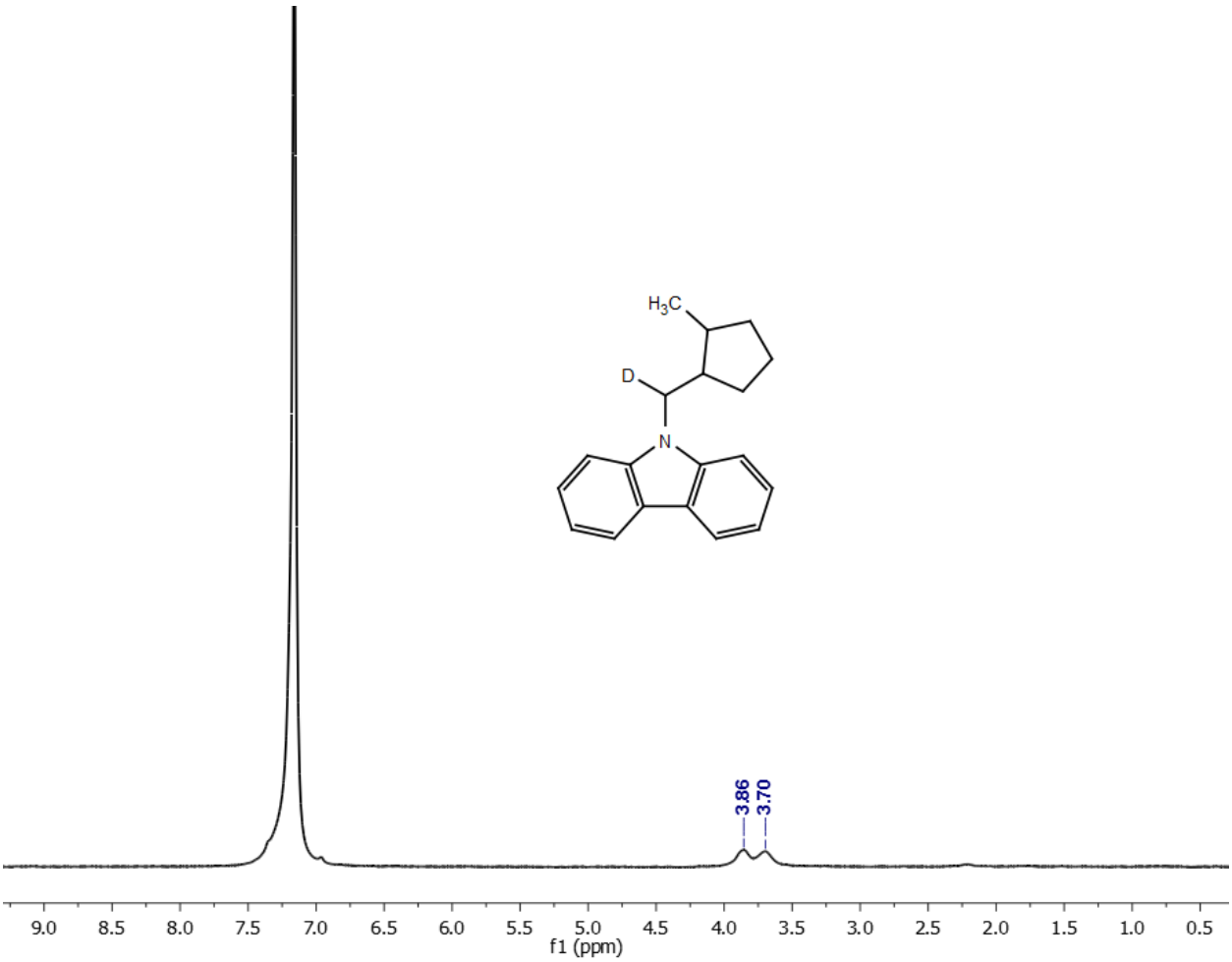

Figure S33: ^{2}H NMR spectrum of 9-((2-methylcyclopentyl)methyl-d)-9H-carbazole (C_6H_6, 61 MHz, rt).

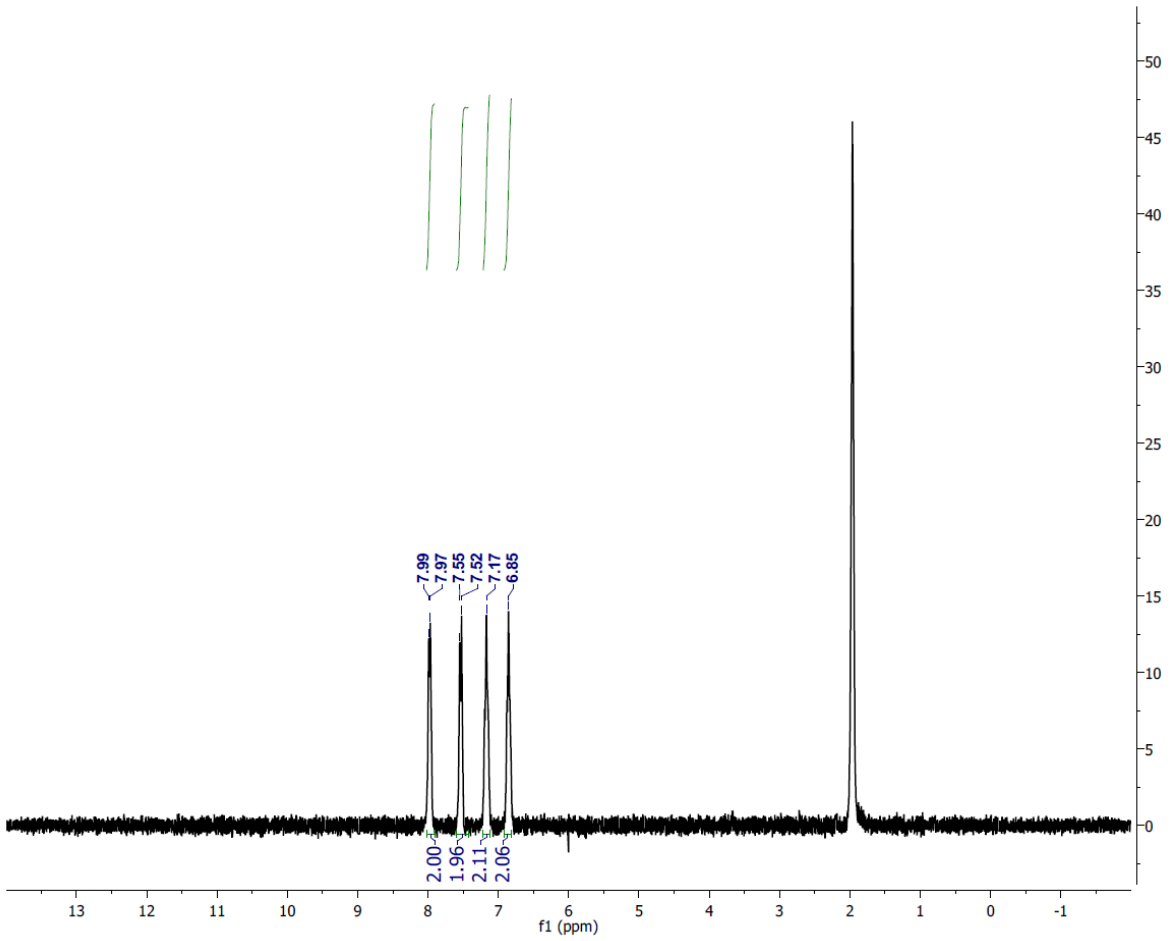

Figure S34: ^{1}H NMR spectrum lithium carbazolide (CD_3CN, 300 MHz, rt).

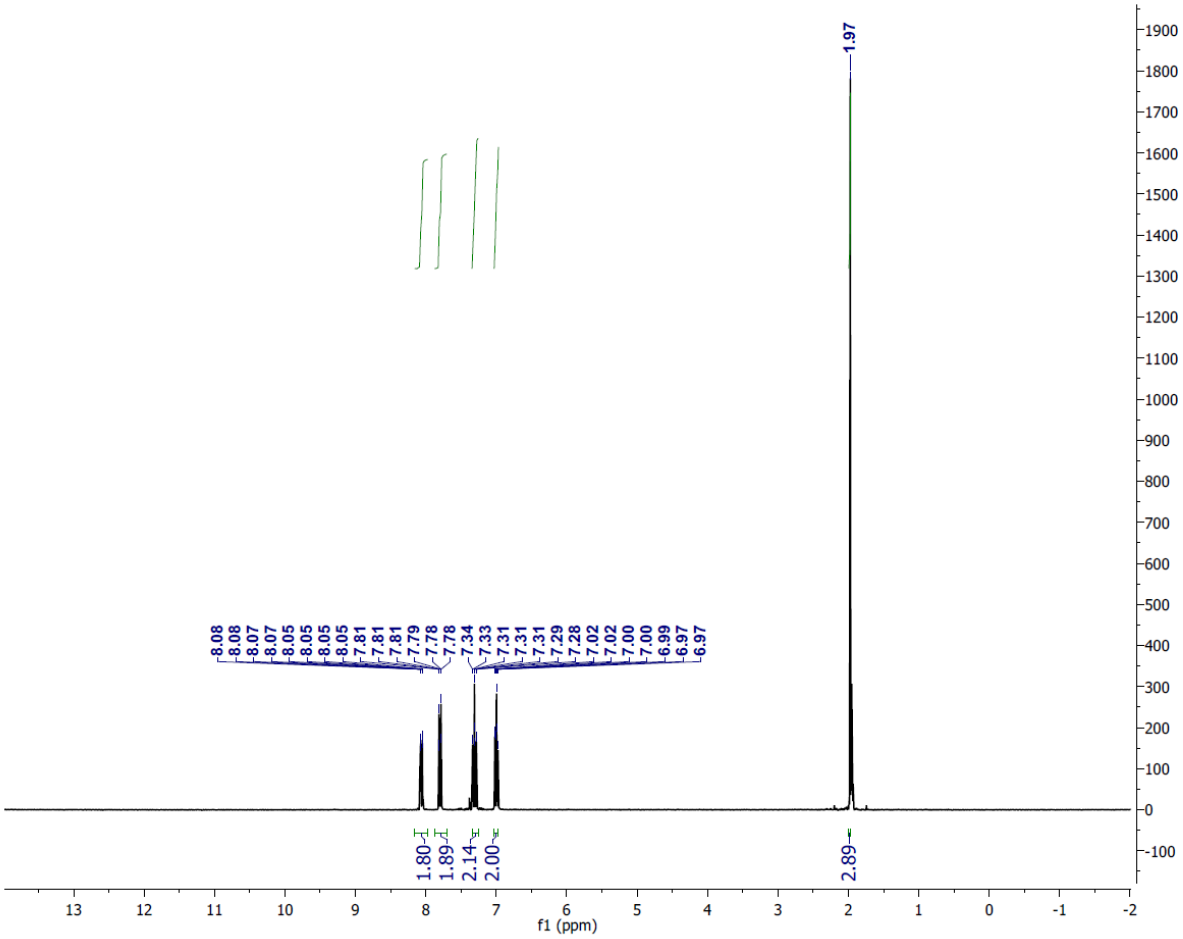

Figure S35: ^{1}H NMR spectrum Li(MeCN)[Cu(carbazolide)$_2$] (CD_3CN, 300 MHz, rt).

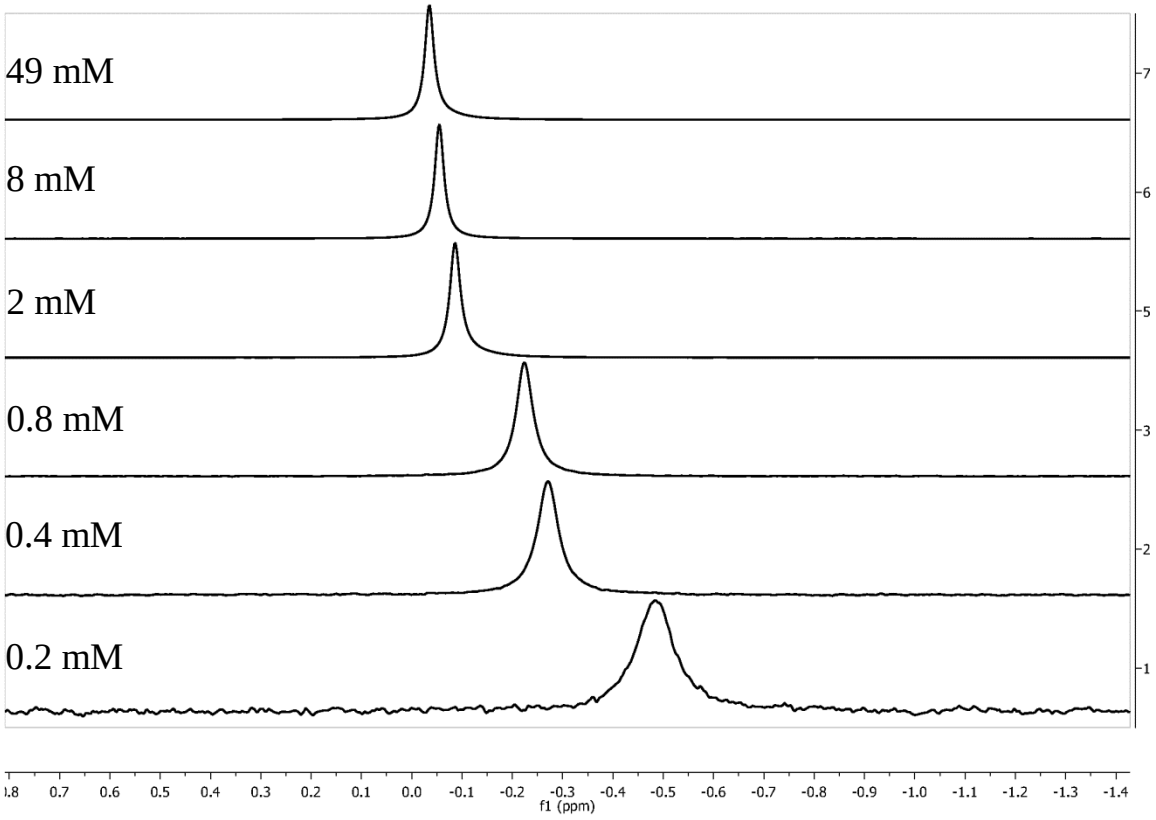

Figure S36: ^{7}Li NMR of lithium carbazolide at various concentrations (CD_3CN, rt, 194 MHz).

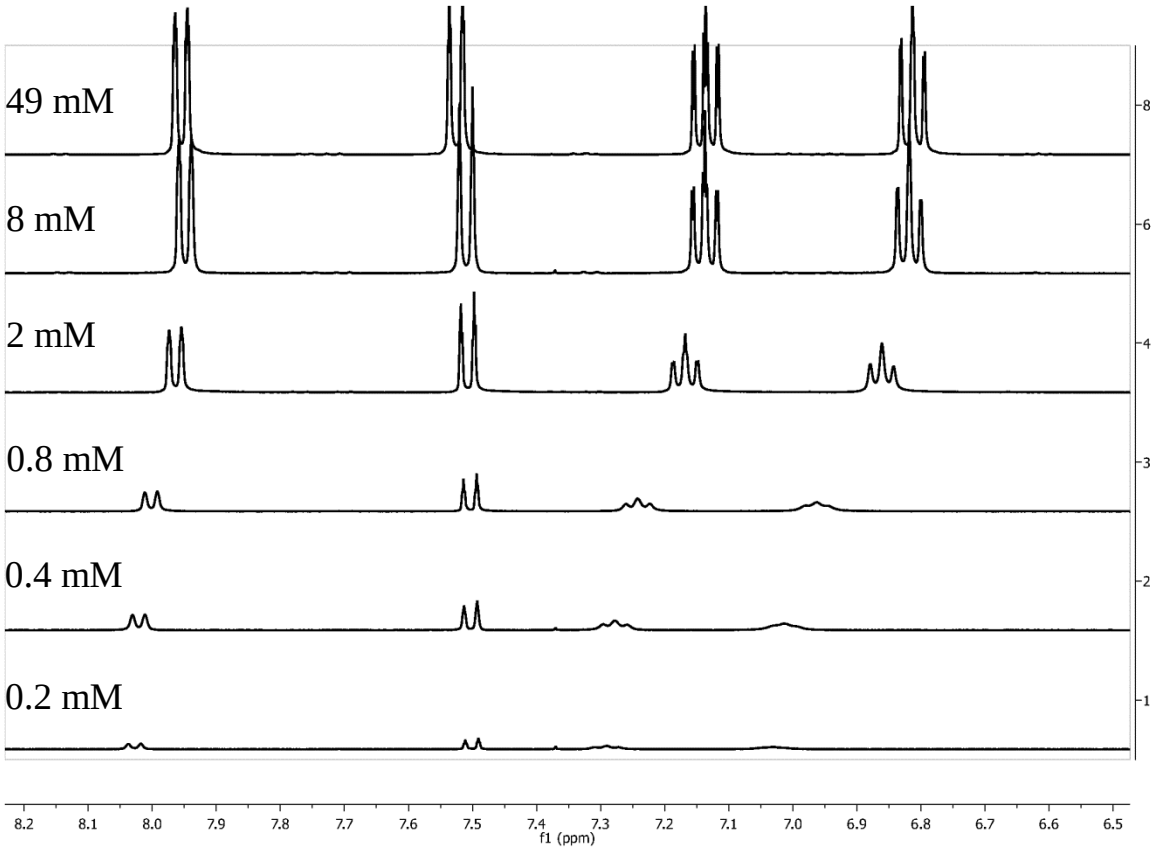

Figure S37: ^{1}H NMR of lithium carbazolide at various concentrations (CD_3CN, rt, 500 MHz).

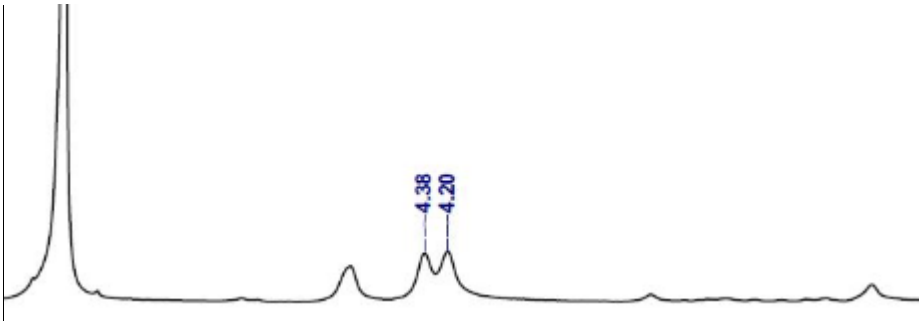

Figure S38: ^{2}H NMR spectrum of a crude reaction mixture of the reaction between (E)-6-bromohept-1-ene-1-d and Li(carb) as depicted in eq 7 of the main text ($CHCl_3$, rt, 61 MHz).

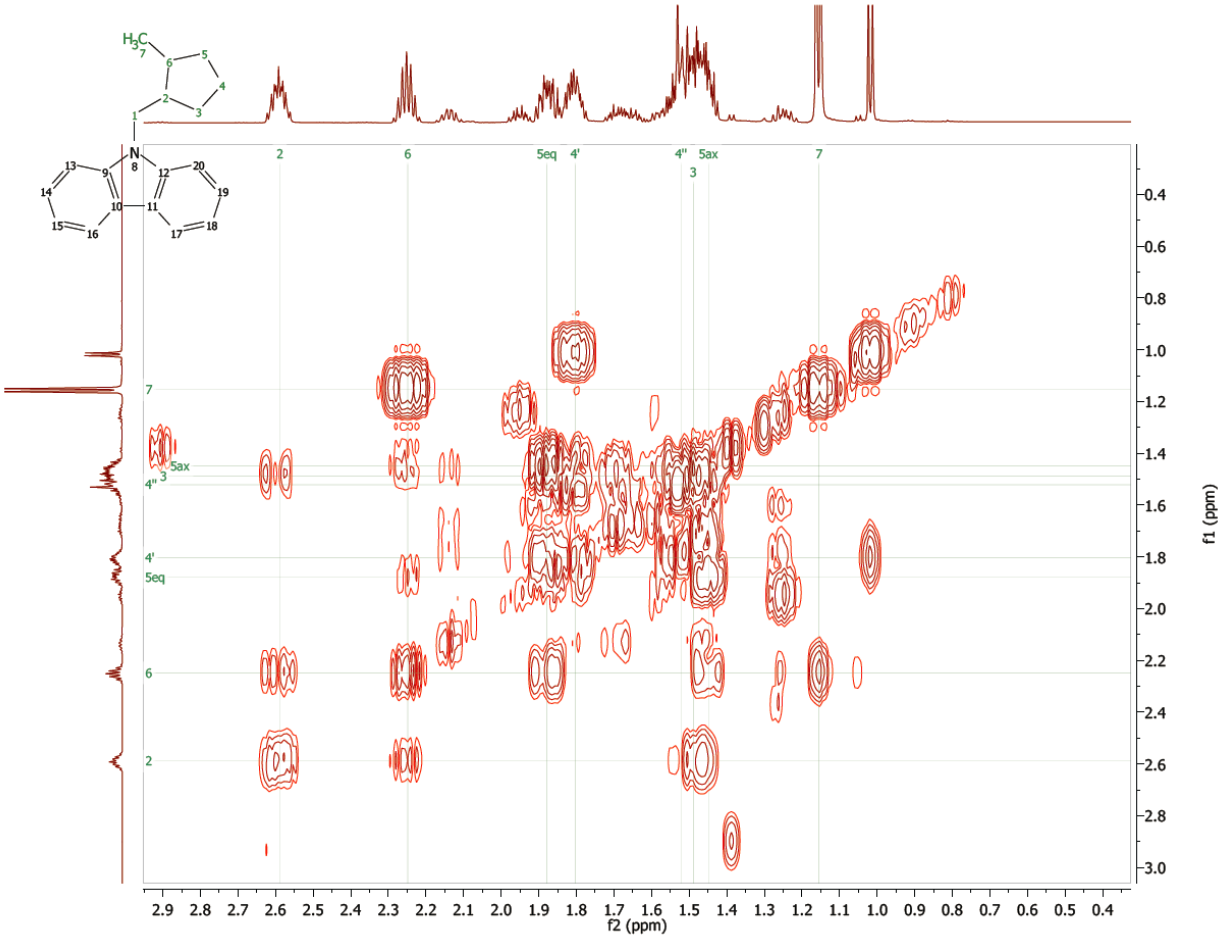

Figure S39: ^{1}H-^{1}H COSY trace of the major diastereomer ($CDCl_3$, rt, 600 MHz) referencing eq 6 of the main text.

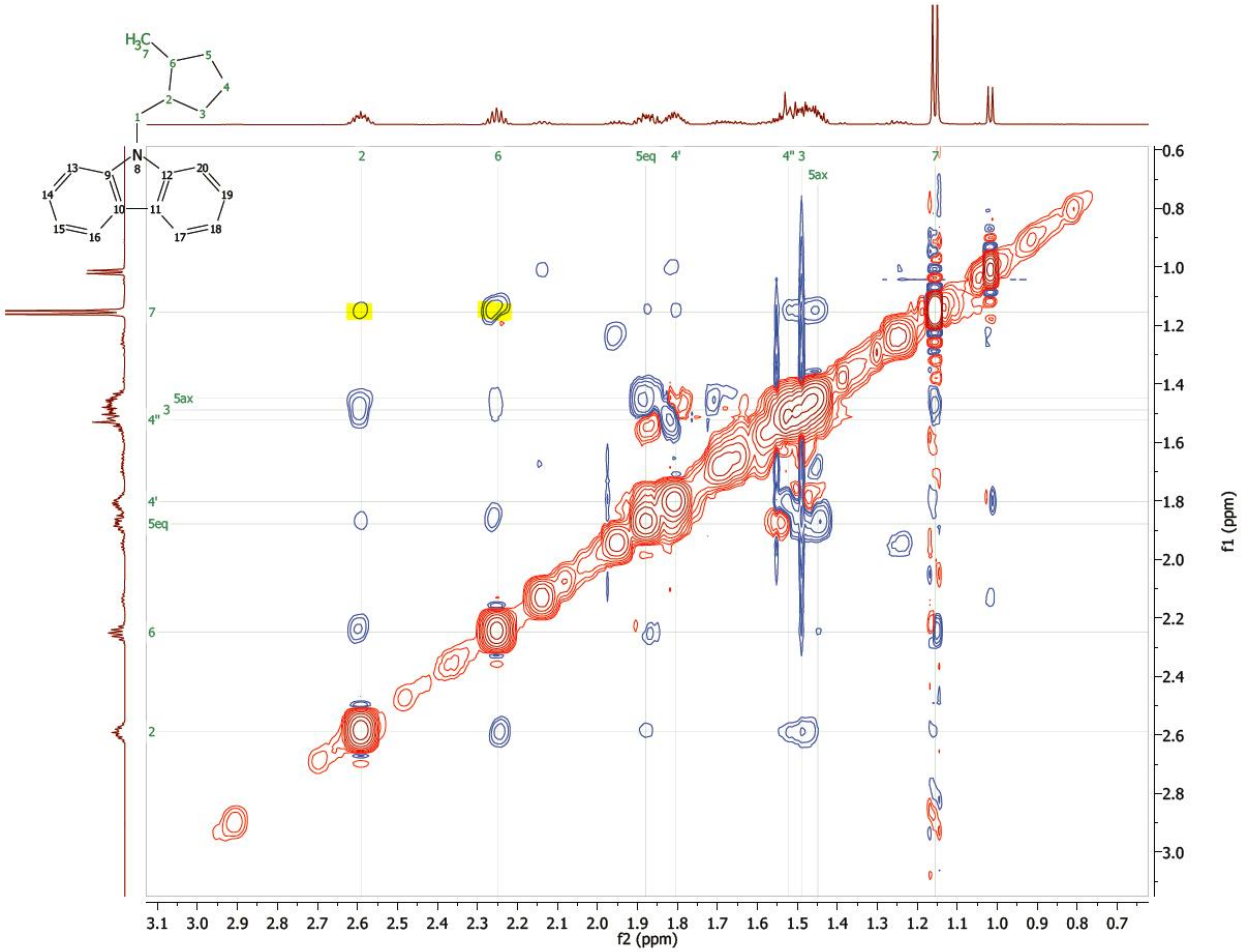

Figure S40: ^{1}H-^{1}H NOESY trace of the major (cis) diastereomer referencing eq 6 of the main text. ($CDCl_3$, rt, 600 MHz). Couplings of the methyl resonances to the methane resonances are highlighted in yellow. The difference in the magnitude of correlation is consistent with the *cis* configuration in a 5-membered ring.

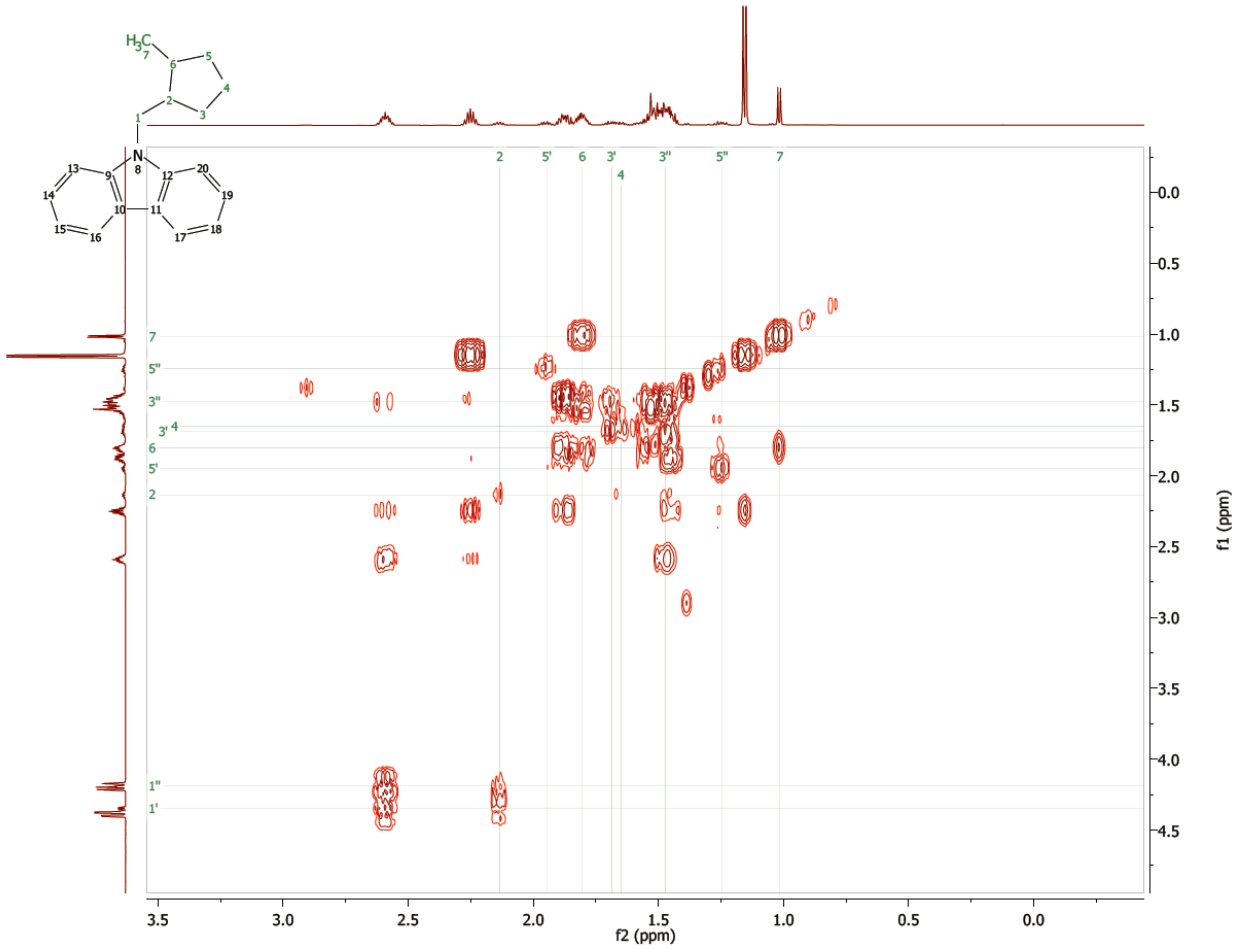

Figure S41: ^{1}H-^{1}H COSY trace of the minor diastereomer ($CDCl_3$, rt, 600 MHz) referencing eq 6 of the main text.

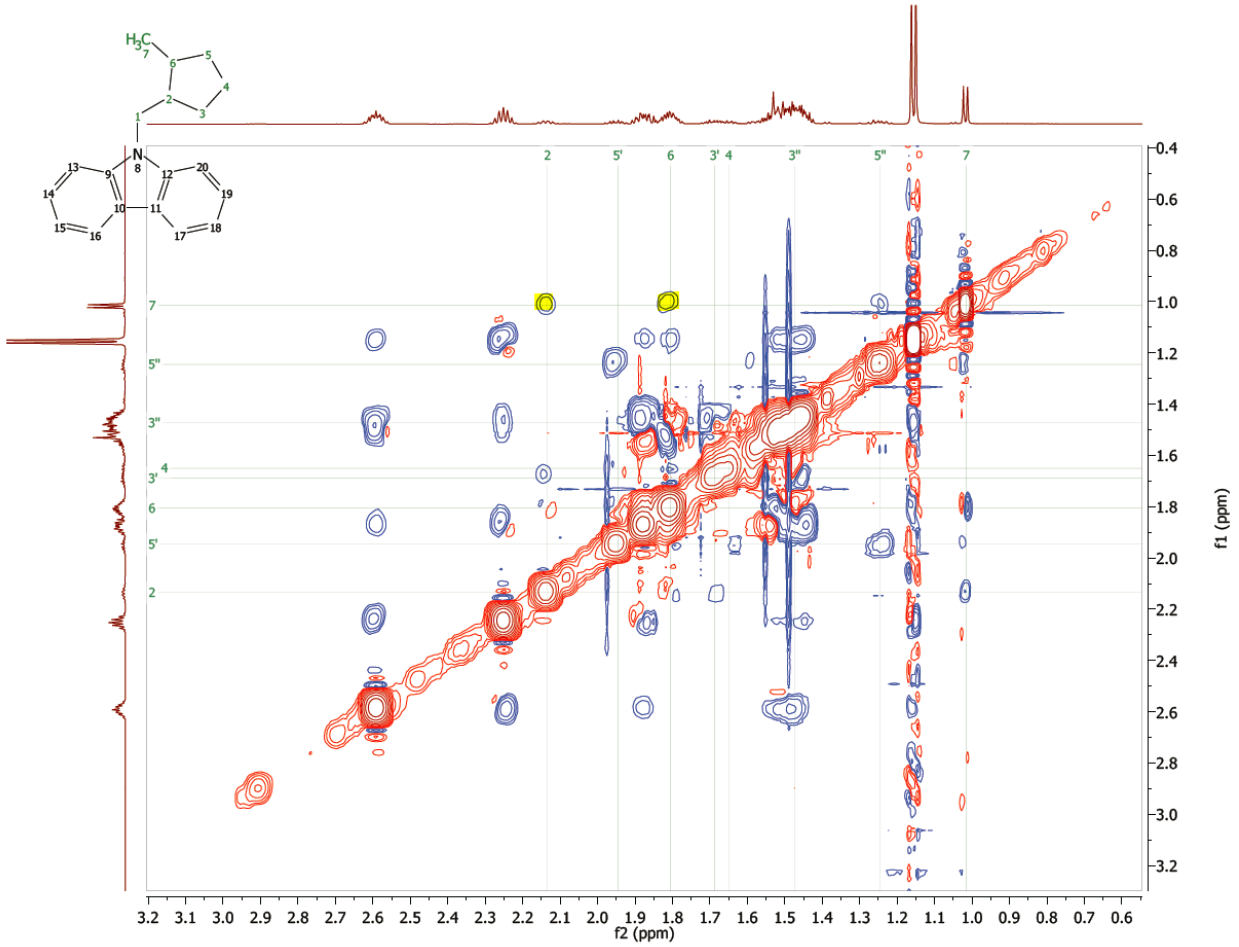

Figure S42: ^{1}H-^{1}H NOESY trace of the minor (*trans*) diastereomer ($CDCl_3$, rt, 600 MHz) referencing eq 6 of the main text. Couplings of the methyl resonances to the methane resonances are highlighted in yellow. Approximately equal magnitude of correlation is consistent with the *trans* configuration in a 5-membered ring.

XIV. X-Ray crystallography data

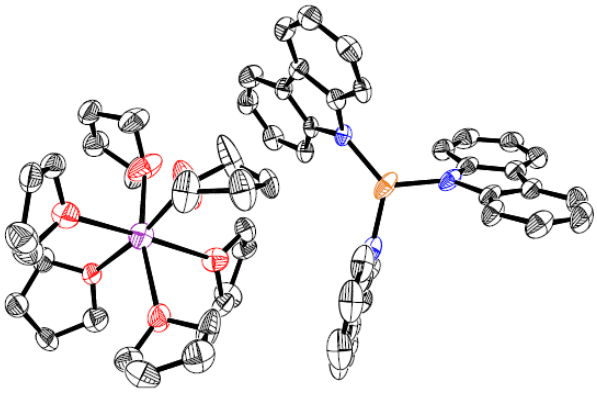

Table S11: Crystal data and structure refinement for $[K(THF)_6][Cu(carbazolide)_3]$

Identification code	$[K(THF)_6][Cu(carbazolide)_3]$
Empirical formula	$C_{40}H_{44}Cu_{0.67}K_{0.67}N_2O_4$
Formula weight	685.20
Temperature/K	100.05
Crystal system	monoclinic
Space group	$P2_1/n$
a/Å	12.9317(5)
b/Å	22.3762(9)
c/Å	18.9484(6)
α/°	90
β/°	104.763(2)
γ/°	90
Volume/Å^3	5301.9(3)
Z	6
ρ_{calc}g/cm^3	1.288
μ/mm^{-1}	1.709
F(000)	2172.0
Radiation	CuKα (λ = 1.54178)
2Θ range for data collection/°	6.234 to 136.854
Index ranges	$-15 \le h \le 14$, $-26 \le k \le 26$, $-22 \le l \le 22$
Reflections collected	57323
Independent reflections	9697 [R_{int} = 0.1553, R_{sigma} = 0.1076]
Data/restraints/parameters	9697/0/650
Goodness-of-fit on F^2	1.043
Final R indexes [I>=2σ (I)]	R_1 = 0.1065, wR_2 = 0.2568
Final R indexes [all data]	R_1 = 0.1845, wR_2 = 0.3014
Largest diff. peak/hole / e Å^{-3}	1.19/-0.99

Table S12: Fractional atomic coordinates ($\times 10^4$) and equivalent isotropic displacement parameters ($Å^2 \times 10^3$) for [K(THF)$_6$][Cu(carbazolide)$_3$]. U_{eq} is defined as 1/3 of the trace of the orthogonalised U_{IJ} tensor.

Atom	*x*	*y*	*z*	U(eq)
Cu01	4786.3(8)	5173.8(6)	2403.2(5)	46.4(4)
K002	155.6(14)	6827.8(8)	2586.4(10)	56.2(5)
N003	3640(4)	4749(2)	2613(2)	27.6(12)
O004	2166(4)	6796(2)	3057(3)	48.4(13)
O005	-1816(4)	6897(2)	1959(3)	53.1(14)
O006	724(4)	7682(2)	1949(3)	55.6(15)
N007	4909(4)	6011(3)	2337(3)	43.7(16)
O008	-10(4)	7497(2)	3587(4)	72.9(19)
N009	6048(4)	4818(3)	2281(3)	38.9(14)
O00A	213(5)	5984(3)	3441(3)	75(2)
C00B	3364(5)	4737(3)	3280(3)	28.4(14)
C00C	2868(5)	4412(3)	2140(3)	29.5(14)
C00D	5478(5)	6373(3)	2893(3)	37.1(17)
C00E	2100(5)	4189(3)	2483(3)	30.7(14)
O00F	158(6)	6072(3)	1667(3)	91(2)
C00G	2432(5)	4405(3)	3231(3)	32.1(15)
C00H	6513(5)	4868(3)	1692(3)	38.1(17)
C00I	6795(6)	4508(3)	2805(4)	38.6(17)
C00J	2802(5)	4274(3)	1414(3)	34.4(16)
C00K	6090(5)	6201(3)	3587(3)	36.5(16)
C00L	6561(5)	6641(3)	4072(4)	39.3(17)
C00M	5390(5)	6980(3)	2709(4)	37.2(17)
C00N	6450(5)	7238(4)	3895(4)	41.1(18)
C00O	7509(6)	4587(3)	1832(4)	40.1(18)
C00P	4714(5)	7000(4)	1960(3)	42.6(19)
C00Q	7705(6)	4357(3)	2562(4)	39.4(17)
C00R	4451(5)	6403(4)	1776(4)	49(2)
C00S	3891(5)	5008(3)	3936(3)	33.5(16)
C00T	1966(6)	3931(3)	1042(4)	43.2(18)
C00U	5877(5)	7407(3)	3205(4)	40.4(17)
C00V	3472(6)	4940(3)	4531(4)	42.9(18)
C00W	1264(5)	3840(3)	2100(4)	41.3(17)
C00X	6067(6)	5129(4)	1004(3)	41.9(18)
C00Y	2023(6)	4343(3)	3844(4)	46.3(19)
C00Z	2561(6)	4608(4)	4480(4)	48(2)
C010	8071(7)	4574(4)	1294(4)	50(2)
C011	8445(6)	3869(3)	3700(4)	48.9(19)

C012	1198(6)	3711(3)	1378(4)	43.5(18)
C013	6630(7)	5103(4)	489(4)	53(2)
C014	8528(6)	4036(3)	3013(4)	49.1(19)
C015	2794(6)	6294(3)	3376(4)	43.3(18)
C016	6724(6)	4345(3)	3504(4)	45.4(19)
C017	-2539(6)	6409(3)	1671(4)	46.6(19)
C018	2827(6)	7310(4)	3272(4)	46.6(19)
C019	7544(7)	4032(4)	3943(4)	53(2)
C01A	-273(6)	8494(3)	3917(5)	56(2)
C01B	3448(6)	6519(3)	4137(4)	49.0(19)
C01C	-1312(6)	8185(3)	3617(4)	50(2)
C01D	-3206(6)	6635(4)	921(4)	51(2)
C01E	3795(6)	6253(5)	1082(4)	58(2)
C01F	4340(6)	7451(4)	1465(4)	57(2)
C01G	7615(7)	4828(4)	625(4)	59(2)
C01H	310(7)	8261(4)	1768(4)	52(2)
C01I	-2981(7)	7298(4)	924(5)	64(2)
C01J	3402(7)	7182(4)	4060(4)	57(2)
C01K	538(7)	8046(4)	3803(5)	58(2)
C01L	3700(7)	7298(5)	781(4)	64(3)
C01M	3441(7)	6724(5)	600(4)	65(3)
C01N	-460(7)	5480(4)	3290(5)	68(3)
C01O	-1150(7)	5547(4)	3839(5)	59(2)
C01P	174(7)	8314(4)	953(4)	59(2)
C01Q	-471(7)	5874(4)	4459(4)	60(2)
C01R	-1045(6)	7537(4)	3727(5)	58(2)
C01S	-2412(7)	7433(4)	1704(4)	61(2)
C01T	1012(8)	7904(5)	813(4)	69(3)
C01U	546(7)	5956(5)	555(4)	70(3)
C01V	-285(7)	6185(5)	905(4)	69(3)
C01W	1496(7)	7605(5)	1518(4)	73(3)
C01X	526(7)	6049(5)	4223(4)	69(3)
C01Y	925(10)	5623(6)	1747(5)	107(5)
C01Z	963(18)	5441(9)	1012(7)	54(6)
C01{	1510(30)	5740(18)	1300(20)	64(12)

Table S13: Anisotropic displacement parameters ($Å^2×10^3$) for $[K(THF)_6][Cu(carbazolide)_3]$. The anisotropic displacement factor exponent takes the form: $-2\pi^2[h^2a^{*2}U_{11}+2hka^*b^*U_{12}+\ldots]$.

Atom	U_{11}	U_{22}	U_{33}	U_{23}	U_{13}	U_{12}
Cu01	38.7(6)	79.6(9)	24.3(5)	-9.1(5)	13.8(4)	-23.1(6)

K002	48.5(10)	57.0(11)	63.9(12)	1.4(9)	15.6(9)	0.1(8)
N003	26(3)	38(3)	19(2)	0(2)	7(2)	1(2)
O004	44(3)	52(3)	43(3)	-2(3)	-2(2)	-7(2)
O005	56(3)	50(3)	53(3)	-1(3)	12(3)	0(3)
O006	57(3)	61(4)	59(3)	19(3)	34(3)	14(3)
N007	28(3)	74(5)	29(3)	-15(3)	7(2)	-13(3)
O008	52(3)	37(3)	147(6)	-23(3)	56(4)	-6(3)
N009	43(3)	53(4)	25(3)	-6(3)	16(3)	-20(3)
O00A	92(5)	96(5)	50(3)	-21(3)	39(3)	-49(4)
C00B	25(3)	35(4)	26(3)	4(3)	8(3)	9(3)
C00C	29(3)	33(4)	24(3)	3(3)	2(3)	6(3)
C00D	20(3)	66(5)	29(3)	-5(3)	14(3)	-2(3)
C00E	26(3)	37(4)	28(3)	7(3)	3(3)	2(3)
O00F	113(5)	126(6)	36(3)	5(3)	23(3)	73(5)
C00G	26(3)	39(4)	30(3)	4(3)	6(3)	5(3)
C00H	43(4)	46(4)	29(4)	-14(3)	16(3)	-23(4)
C00I	44(4)	41(4)	33(4)	-12(3)	14(3)	-19(3)
C00J	31(4)	43(4)	28(3)	1(3)	7(3)	13(3)
C00K	26(3)	56(5)	29(3)	-5(3)	9(3)	-8(3)
C00L	26(4)	61(5)	29(4)	2(3)	3(3)	-1(3)
C00M	21(3)	57(5)	34(4)	-5(4)	8(3)	6(3)
C00N	26(4)	60(5)	37(4)	-12(4)	6(3)	5(3)
C00O	46(4)	45(4)	33(4)	-19(3)	18(3)	-20(3)
C00P	21(3)	82(6)	24(4)	-6(4)	5(3)	12(4)
C00Q	46(4)	41(4)	32(4)	-16(3)	12(3)	-15(4)
C00R	28(4)	91(7)	30(4)	4(4)	11(3)	6(4)
C00S	26(3)	45(4)	27(3)	2(3)	3(3)	7(3)
C00T	49(4)	44(4)	31(4)	-7(3)	-1(3)	10(4)
C00U	31(4)	49(4)	43(4)	0(4)	11(3)	9(3)
C00V	49(4)	55(5)	23(3)	-1(3)	6(3)	9(4)
C00W	33(4)	48(5)	44(4)	0(4)	11(3)	-1(3)
C00X	39(4)	63(5)	25(3)	-8(3)	12(3)	-13(4)
C00Y	55(5)	55(5)	32(4)	5(4)	18(3)	-9(4)
C00Z	50(5)	60(5)	41(4)	13(4)	22(4)	6(4)
C010	58(5)	59(5)	39(4)	-11(4)	25(4)	-3(4)
C011	51(5)	45(5)	50(5)	-6(4)	10(4)	-11(4)
C012	35(4)	43(4)	46(4)	-3(4)	-1(3)	3(3)
C013	60(5)	72(6)	28(4)	-8(4)	15(4)	-23(5)
C014	57(5)	47(5)	49(5)	-13(4)	23(4)	-8(4)
C015	42(4)	46(4)	41(4)	1(4)	7(3)	11(3)
C016	60(5)	47(5)	34(4)	-5(4)	22(4)	-10(4)

C017	48(4)	47(5)	50(4)	-4(4)	23(4)	-5(4)
C018	35(4)	57(5)	49(4)	5(4)	13(3)	-8(4)
C019	71(6)	54(5)	38(4)	-4(4)	18(4)	-23(4)
C01A	53(5)	36(4)	80(6)	-10(4)	19(4)	7(4)
C01B	41(4)	51(5)	51(5)	0(4)	4(4)	-12(4)
C01C	50(5)	48(5)	54(5)	6(4)	17(4)	7(4)
C01D	40(4)	60(5)	58(5)	4(4)	21(4)	6(4)
C01E	35(4)	105(7)	32(4)	-22(5)	5(3)	-1(4)
C01F	37(4)	94(7)	39(4)	-1(5)	11(4)	21(4)
C01G	70(6)	82(6)	37(4)	-18(4)	34(4)	-16(5)
C01H	58(5)	51(5)	48(5)	2(4)	15(4)	-5(4)
C01I	76(6)	58(6)	61(6)	8(4)	20(5)	10(5)
C01J	66(5)	55(5)	42(4)	-3(4)	0(4)	3(4)
C01K	54(5)	56(5)	64(5)	-4(4)	16(4)	-4(4)
C01L	51(5)	107(8)	30(4)	4(5)	2(4)	29(5)
C01M	45(5)	122(9)	26(4)	0(5)	4(4)	24(5)
C01N	76(6)	74(6)	62(5)	-41(5)	32(5)	-39(5)
C01O	52(5)	62(5)	71(6)	-16(5)	32(4)	-13(4)
C01P	79(6)	48(5)	42(5)	3(4)	-1(4)	6(4)
C01Q	67(6)	66(6)	57(5)	-5(4)	31(4)	-9(5)
C01R	51(5)	55(5)	79(6)	12(5)	37(4)	6(4)
C01S	73(6)	55(5)	60(5)	-12(4)	25(5)	-3(5)
C01T	84(7)	83(7)	46(5)	18(5)	28(5)	6(5)
C01U	79(6)	100(8)	37(4)	-2(5)	24(4)	28(6)
C01V	53(5)	121(9)	34(4)	2(5)	9(4)	14(5)
C01W	49(5)	132(9)	47(5)	29(5)	27(4)	17(5)
C01X	48(5)	116(9)	45(5)	-17(5)	13(4)	-17(5)
C01Y	142(10)	140(11)	38(5)	12(6)	23(6)	111(9)
C01Z	71(12)	55(10)	37(8)	-3(7)	17(7)	22(9)
C01{	48(19)	50(20)	100(30)	10(20)	31(19)	25(15)

Table S14: Hydrogen atom coordinates (Å×10^4) and isotropic displacement parameters (Å^2×10^3) for [K(THF)$_6$][Cu(carbazolide)$_3$].

Atom	*x*	*y*	*z*	U(eq)
H00J	3325	4415	1183	41
H00K	6176	5791	3719	44
H00L	6976	6528	4543	47
H00N	6765	7532	4246	49
H00S	4524	5234	3971	40
H00T	1905	3839	543	52
H00U	5819	7817	3073	49

H00V	3816	5125	4981	51
H00W	744	3691	2330	50
H00X	5387	5318	903	50
H00Y	1387	4123	3817	56
H00Z	2298	4561	4902	58
H010	8756	4392	1387	59
H011	9001	3642	4009	59
H012	626	3472	1107	52
H013	6338	5279	25	63
H014	9143	3932	2853	59
H01A	3275	6166	3073	52
H01B	2330	5953	3429	52
H016	6114	4451	3670	54
H01C	-3007	6319	1999	56
H01D	-2136	6043	1614	56
H01E	2390	7677	3232	56
H01F	3341	7355	2968	56
H019	7507	3922	4421	64
H01G	-168	8586	4442	67
H01H	-231	8870	3649	67
H01I	3119	6386	4528	59
H01J	4195	6374	4247	59
H01K	-1598	8277	3092	60
H01L	-1845	8305	3883	60
H01M	-2982	6434	519	62
H01N	-3978	6560	864	62
H0BA	3604	5851	950	69
H1BA	4515	7857	1587	68
H2BA	7985	4814	252	71
H01O	812	8568	2033	63
H01P	-385	8310	1890	63
H01Q	-2523	7394	593	77
H01R	-3654	7529	770	77
H01S	4132	7352	4177	68
H01T	3007	7358	4393	68
H01U	874	8188	3419	69
H01V	1105	7991	4260	69
H3BA	3440	7604	434	77
H4BA	3002	6638	128	78
H01W	-219	5084	3145	82
H01X	-1810	5775	3621	71

H01Y	-1349	5151	3995	71
H01Z	-549	8185	680	71
H	294	8730	814	71
H01	-283	5616	4899	72
HA	-846	6233	4572	72
H0AA	-1197	7318	4150	69
H1AA	-1927	7780	1733	74
HB	-2930	7520	1995	74
H2AA	689	7606	435	83
HC	1560	8133	645	83
H3AA	228	5835	42	85
HD	1110	6258	568	85
HE	804	6273	278	85
HF	277	5615	226	85
H4AA	-1025	6029	697	83
H5AA	2249	7723	1762	88
H6AA	1256	5931	4515	83
H7AA	599	5273	1939	128
H8AA	1706	5350	995	65
HG	514	5083	852	65
H9AA	1897	5381	1194	76
HH	2029	6064	1480	76

Table S15: Bond angles for $[K(THF)_6][Cu(carbazolide)_3]$.

Atom	Atom	Atom	Angle/°	Atom	Atom	Atom	Angle/°
N007	Cu01	N003	126.7(2)	N007	C00D	C00M	112.7(6)
N009	Cu01	N003	124.4(2)	C00M	C00D	C00K	119.4(6)
N009	Cu01	N007	108.8(2)	C00C	C00E	C00G	105.4(5)
O004	K002	O005	172.63(17)	C00W	C00E	C00C	120.4(6)
O004	K002	C01N	99.0(2)	C00W	C00E	C00G	134.2(6)
O004	K002	C01R	112.86(19)	C01V	O00F	K002	121.7(6)
O004	K002	C01V	103.31(19)	C01Y	O00F	K002	123.8(6)
O004	K002	C01W	66.16(18)	C01Y	O00F	C01V	109.1(6)
O004	K002	C01X	77.03(18)	C00B	C00G	C00E	106.0(5)
O004	K002	C01Y	75.3(3)	C00B	C00G	C00Y	119.9(6)
O005	K002	C01N	86.1(2)	C00Y	C00G	C00E	134.1(6)
O005	K002	C01R	72.44(19)	N009	C00H	C00X	127.7(7)
O005	K002	C01V	71.19(19)	C00O	C00H	N009	112.0(6)
O005	K002	C01W	106.87(19)	C00O	C00H	C00X	120.1(6)
O005	K002	C01X	110.06(19)	N009	C00I	C00Q	112.0(6)
O005	K002	C01Y	102.0(2)	N009	C00I	C016	127.4(7)

O006	K002	O004	77.68(18)	C016	C00I	C00Q	120.6(7)
O006	K002	O005	96.48(18)	C00T	C00J	C00C	118.4(6)
O006	K002	O00A	161.2(2)	C00L	C00K	C00D	118.4(7)
O006	K002	C01N	170.4(2)	C00N	C00L	C00K	122.0(7)
O006	K002	C01R	101.11(19)	C00D	C00M	C00P	105.2(6)
O006	K002	C01V	82.5(2)	C00U	C00M	C00D	120.7(6)
O006	K002	C01W	21.1(2)	C00U	C00M	C00P	134.2(7)
O006	K002	C01X	146.3(2)	C00L	C00N	C00U	119.6(7)
O006	K002	C01Y	103.0(3)	C00H	C00O	C00Q	105.8(6)
O008	K002	O004	91.64(18)	C010	C00O	C00H	119.9(7)
O008	K002	O005	92.87(19)	C010	C00O	C00Q	134.3(7)
O008	K002	O006	90.1(2)	C00R	C00P	C00M	105.0(7)
O008	K002	O00A	87.3(2)	C01F	C00P	C00M	134.5(8)
O008	K002	C01N	99.1(2)	C01F	C00P	C00R	120.5(7)
O008	K002	C01R	22.38(19)	C00I	C00Q	C00O	105.7(6)
O008	K002	C01V	161.4(2)	C014	C00Q	C00I	119.8(7)
O008	K002	C01W	107.5(2)	C014	C00Q	C00O	134.4(7)
O008	K002	C01X	68.8(2)	N007	C00R	C00P	112.6(6)
O008	K002	C01Y	158.8(2)	N007	C00R	C01E	126.9(9)
O00A	K002	O004	83.75(19)	C00P	C00R	C01E	120.6(8)
O00A	K002	O005	102.3(2)	C00V	C00S	C00B	118.4(6)
O00A	K002	C01N	19.58(19)	C00J	C00T	C012	121.5(7)
O00A	K002	C01R	83.2(2)	C00M	C00U	C00N	119.9(7)
O00A	K002	C01V	105.1(2)	C00Z	C00V	C00S	120.7(7)
O00A	K002	C01W	146.3(2)	C012	C00W	C00E	118.8(7)
O00A	K002	C01X	20.2(2)	C013	C00X	C00H	118.6(7)
O00A	K002	C01Y	74.8(2)	C00Z	C00Y	C00G	118.4(7)
O00F	K002	O004	92.6(2)	C00Y	C00Z	C00V	122.0(7)
O00F	K002	O005	83.7(2)	C01G	C010	C00O	118.8(8)
O00F	K002	O006	97.7(2)	C014	C011	C019	120.5(8)
O00F	K002	O008	171.8(2)	C00W	C012	C00T	120.4(7)
O00F	K002	O00A	86.1(2)	C00X	C013	C01G	121.5(7)
O00F	K002	C01N	73.3(2)	C00Q	C014	C011	119.3(7)
O00F	K002	C01R	151.0(2)	O004	C015	C01B	104.6(6)
O00F	K002	C01V	21.0(2)	C019	C016	C00I	118.9(7)
O00F	K002	C01W	80.7(3)	O005	C017	C01D	104.6(6)
O00F	K002	C01X	105.4(2)	O004	C018	K002	36.1(3)
O00F	K002	C01Y	19.9(2)	O004	C018	C01J	103.7(6)
C01N	K002	C01X	38.4(2)	C01J	C018	K002	119.5(5)
C01R	K002	C01N	88.5(2)	C016	C019	C011	120.9(7)
C01R	K002	C01V	143.6(2)	C01C	C01A	C01K	103.2(6)

C01R	K002	C01W	121.5(2)	C01J	C01B	C015	103.5(6)
C01R	K002	C01X	69.2(2)	C01A	C01C	C01R	104.2(6)
C01R	K002	C01Y	155.7(3)	C01I	C01D	C017	104.9(6)
C01V	K002	C01N	89.6(2)	C01M	C01E	C00R	116.7(9)
C01V	K002	C01W	69.7(2)	C00P	C01F	C01L	118.4(9)
C01V	K002	C01X	125.0(3)	C010	C01G	C013	121.1(7)
C01W	K002	C01N	149.5(2)	O006	C01H	C01P	105.0(6)
C01W	K002	C01X	143.0(2)	C01S	C01I	C01D	104.3(7)
C01Y	K002	C01N	67.3(3)	C01B	C01J	C018	106.4(6)
C01Y	K002	C01V	39.5(2)	O008	C01K	K002	33.8(3)
C01Y	K002	C01W	82.8(3)	O008	C01K	C01A	107.6(6)
C01Y	K002	C01X	91.7(2)	C01A	C01K	K002	128.5(5)
C00B	N003	Cu01	126.6(4)	C01M	C01L	C01F	121.5(9)
C00C	N003	Cu01	127.9(4)	C01L	C01M	C01E	122.3(8)
C00C	N003	C00B	105.5(5)	O00A	C01N	K002	36.1(4)
C015	O004	K002	126.5(4)	O00A	C01N	C01O	102.6(6)
C015	O004	C018	106.2(5)	C01O	C01N	K002	113.8(6)
C018	O004	K002	124.4(4)	C01Q	C01O	C01N	105.0(6)
C017	O005	K002	127.4(4)	C01T	C01P	C01H	103.5(6)
C01S	O005	K002	126.7(5)	C01O	C01Q	C01X	105.7(6)
C01S	O005	C017	105.2(6)	O008	C01R	K002	41.0(4)
C01H	O006	K002	133.5(4)	O008	C01R	C01C	103.2(6)
C01H	O006	C01W	104.1(6)	C01C	C01R	K002	119.7(5)
C01W	O006	K002	121.1(5)	O005	C01S	C01I	104.3(6)
C00D	N007	Cu01	124.7(5)	C01W	C01T	C01P	106.0(7)
C00D	N007	C00R	104.6(7)	C01V	C01U	C01{	101.0(11)
C00R	N007	Cu01	130.7(5)	C01Z	C01U	C01V	101.9(9)
C01K	O008	K002	127.5(5)	O00F	C01V	K002	37.3(4)
C01K	O008	C01R	108.2(6)	O00F	C01V	C01U	103.9(7)
C01R	O008	K002	116.6(5)	C01U	C01V	K002	126.4(6)
C00H	N009	Cu01	128.7(5)	O006	C01W	K002	37.8(4)
C00I	N009	Cu01	126.3(4)	O006	C01W	C01T	105.1(7)
C00I	N009	C00H	104.4(6)	C01T	C01W	K002	126.6(6)
C01N	O00A	K002	124.3(5)	O00A	C01X	K002	36.4(4)
C01N	O00A	C01X	106.7(6)	O00A	C01X	C01Q	103.8(6)
C01X	O00A	K002	123.4(5)	C01Q	C01X	K002	117.2(6)
N003	C00B	C00G	111.4(5)	O00F	C01Y	K002	36.3(4)
C00S	C00B	N003	128.1(6)	O00F	C01Y	C01Z	107.1(8)
C00S	C00B	C00G	120.4(6)	C01Z	C01Y	K002	138.5(8)
N003	C00C	C00E	111.7(5)	C01{	C01Y	K002	116(2)
N003	C00C	C00J	127.9(6)	C01{	C01Y	O00F	107.5(14)

C00J	C00C	C00E	120.3(6)	C01U	C01Z	C01Y	104.4(11)
N007	C00D	C00K	127.9(7)	C01Y	C01{	C01U	100(2)

XV. References

(1) Tsuda, T.; Yazawa, T.; Watanabe, K.; Fujii, T.; Saegusa, T. *J. Org. Chem.* **1981**, *46*, 192–194.

(2) González-Bobes, F.; Fu, G. C. *J. Am. Chem. Soc.* **2006**, *128*, 5360–5361.

(3) Stoll, S.; Schweiger, A. *J. Magn. Reson.* **2006**, *178*, 42–55.

(4) (a) Kimura, T.; Lee, J. C.; Gray, H. B.; Winkler, J. R. *Proc. Natl. Acad. Sci. U. S. A.* **2009**, *106*, 7834–7839. (b) Yamada, S.; Bouley Ford, N. D.; Keller, G. E.; Ford, W. C.; Gray, H. B.; Winkler, J. R. *Proc. Natl. Acad. Sci. U. S. A.* **2013**, *110*, 1606–1610.

(5) Leijondahl, K.; Borén, L.; Braun, R.; Bäckvall, J.-E. *J. Org. Chem.* **2009**, *74*, 1988–1993.

(6) Sargent, B. T.; Alexanian, E. J. *J. Am. Chem. Soc.* **2016**, *138*, 7520–7523.

(7) Bissember, A. C.; Lundgren, R. J.; Creutz, S. E. Peters, J. C. Fu, G. C. *Angew. Chem. Int. Ed.* **2013**, *52*, 5129–5133.

(8) Dinnebier, R.; Esbak, H.; Olbrich, F.; Behrens, U. *Organometallics* **2007**, *26*, 2604–2608.

(9) (a) Murov, S. L.; Carmichael, I.; Hug, G. L. Handbook of Photochemistry; CRC Press: New York, 1993; pp 298−313. (b) Bolton, J. R.; Stefan, M. I.; Shaw, P.-S.; Lykke, K. R. *J. Photochem. Photobiol., A* **2011**, *222*, 166−169.

(10) Wu, A.; Mader, E. A.; Datta, A.; Hrovat, D. A.; Borden, W. T.; Mayer, J. M. *J. Am. Chem. Soc.* **2009**, *131*, 11985–11997.

(11) Neese, F. *Wiley Interdiscip. Rev. Comput. Mol. Sci.* **2012**, *2*, 73–78.

(12) Zhao, Y.; Truhlar, D.G. *J. Chem. Phys.* **2006**, *125*, 194101.

(13) Weigend, F.; Furche, F.; Ahlrichs, R. *J. Chem. Phys.* **2003**, *119*, 12753.

(14) Klamt, A; Schüürmann, G. *J. Chem. Soc. Perkin Trans. 2* **1993**, *2*, 799–805.